2020-01-01

Utilizing Zircon (U-Th)/He And 40ar/39ar Thermochronology To Refine The Thermal History Of The Great Unconformity Within New Mexico And Colorado

Jacoup Roiz
University of Texas at El Paso

UTILIZING ZIRCON (U-Th)/He AND $^{40}Ar/^{39}Ar$ THERMOCHRONOLOGY TO REFINE THE THERMAL HISTORY OF THE GREAT UNCONFORMITY WITHIN NEW MEXICO AND COLORADO

JACOUP ROIZ

MASTER'S PROGRAM IN GEOLOGICAL SCIENCES

APPROVED:

Jason Ricketts, Ph.D., Chair

Terry Pavlis, Ph.D.

Karl Karlstrom, Ph.D.

Stephen Crites, Ph.D.
Dean of the Graduate School

UTILIZING ZIRCON (U-Th)/He AND $^{40}Ar/^{39}Ar$ THERMOCHRNOLOGY TO REFINE THE THERMAL HISTORY OF THE GREAT UNCONFORMITY WITHIN NEW MEXICO AND COLORADO

by

JACOUP ROIZ, B.S.

THESIS

Presented to the Faculty of the Graduate School of

The University of Texas at El Paso

in Partial Fulfillment

of the Requirements

for the Degree of

MASTER OF SCIENCE

Department of Geological Sciences

THE UNIVERSITY OF TEXAS AT EL PASO

May 2020

Acknowledgements

I would like to express my deep gratitude towards my committee chair and advisor Dr. Jason Ricketts. His continuous support and motivation, extensive knowledge, and guidance made this thesis project possible.

Additionally, I would like to thank the rest of my committee members, Dr. Terry Pavlis and Dr. Karl Karlstrom, for their constructive suggestions and involvement in the project. I would also like to sincerely thank the entire staff and faculty of the UTEP Geological Sciences department. My two years here were great because of all of you and I could not have asked for a better department.

Finally, I would like to thank my entire family for always supporting every decision I make and motivating me to continue my education. Without your unwavering support I would not have been able to reach this point.

Abstract

The Great Unconformity beneath Paleozoic strata represents 100-1000 m.y. of missing rock record that formed through extensive weathering and erosion. Despite its global extent, the timing of Precambrian crystalline rock exhumation prior to Phanerozoic sediment deposition remains relatively unresolved in many locations. I utilized zircon (U-Th)/He (ZHe) thermochronology in order to constrain the long-term thermal history of Precambrian rocks in Colorado and New Mexico, and test my hypothesis that these units below the Great Unconformity experienced multiple cooling and reheating episodes resulting in a compound surface representing multiple unconformities. In addition to a synthesis of previously reported data in the area, three new samples have been collected within New Mexico and Colorado for ZHe analysis from Santa Fe, Los Pinos Mountains, and Tres Piedras. Results for the ZHe dates range from 31.6-835.06 Ma in Santa Fe, 79.62-863.86 Ma for Los Pinos Mountains, and 47.34-364.73 Ma for Tres Piedras.

HeFTy software was then utilized to create new forward and inverse thermal history models from the compiled ZHe data. Forward models for the samples resulted in ZHe date vs. eU curves that did not correspond to the data. Two inverse models were then completed for each sample and included a gradual cooling and reburial scenario in order to constrain the long-term thermal history of each location. For the Santa Fe, Tres Piedras, and Sandia Mountains samples the gradual cooling scenario is more likely to have occurred. For the Los Pinos Mountains and Front Range, CO locations both the reburial and gradual cooling model remain a possibility. The inverse model results indicate that two scenarios are possible for the five samples analyzed. Scenario one would be that the gradual cooling model occurred for all five locations. While scenario two would be that only the Santa Fe, Tres Piedras, and Sandia Mountains samples

experienced the gradual cooling model while the Los Pinos Mountains and Front Range locations underwent the reburial model. Overall the thermal histories recorded in the inverse models link the cooling to near-surface temperatures to the breakup of supercontinent Rodinia. These new data provide new and important insight into the timescales and processes of continental exhumation during assembly and break-up of supercontinents.

Table of Contents

List of Tables

List of Figures

Chapter 1: Introduction

The Great Unconformity (GU) is a globally significant feature in the rock record and is typically defined as the boundary between Precambrian igneous or metamorphic basement rocks and Phanerozoic sedimentary strata. This rock contact represents between 100 to >1000 m.y. of missing rock record and formed due to weathering and erosion processes (*DeLucia et al.* 2017). Although the GU represents a significant period in the rock record and is a global feature, there is still debate as to whether the formation of this unconformity occurred as one main event, or is a combination of multiple unconformities that culminated in a single composite erosion surface (e.g. *Timmons et al.* 2001).

Understanding the formation of the GU is pivotal to the entire geologic rock record not only due to the vast amount of time this unconformity encompasses, but also because the creation of the GU could have triggered multiple key events in Earth's history. *DeLucia et al.* (2017) linked the weathering and erosion that formed the GU to either breakup of the supercontinent Rodinia or snowball Earth glaciations that occurred between ~ 750 to 550 Ma (*Hoffman et al.* 1998). Subsequently, the GU has also been suggested as a prime contributor to the Cambrian explosion that occurred shortly after (*Peter and Gaines*, 2012). *Peters & Gaines* (2012) state that the discovery of skeletonized crown-group animals in Cambrian sediments that lie above the GU is evidence supporting this relationship because this find adds to an incomplete record of early animal evolution due to a stratigraphic bias. Therefore, uncovering the exact processes that occurred during the formation of the GU is pertinent not only to furthering our understanding of possible tectonic events that resulted in widespread exhumation of basement rocks to Earth's surface, but also for establishing whether this increased weathering and erosion

could have had important implications for early life on Earth. While the age of Phanerozoic strata overlying the GU is generally constrained in most cases, the timing of basement rock exhumation is less well known. In order to evaluate these relationships, the timing of basement exhumation must be refined in order to provide clear insight into the ambiguous history and significance of this feature.

Low-temperature thermochronology offers the capability to record several key aspects of the upper ~8 km of the crust, including the magnitude, timing, and extent of exhumation, depending on the specific system utilized (e.g. *Shaw et al.* 2004; *DeLucia et al.* 2017). Specifically, we utilized new helium diffusion models in zircon, as described in more detail below, to provide new constraints on the timing of GU formation. A general goal of this project is to constrain when Precambrian basement rocks at different locations were exhumed to surface temperatures prior to deposition of Phanerozoic sediment. More specifically, these data are used to test the hypothesis that this erosional contact is a compound surface that represents multiple superimposed unconformities. Figure 1 highlights two possible scenarios that will be explored. Scenario one portrays the GU as a simple unconformity, where a pluton crystallizes at depth during the Precambrian and is overlain by Precambrian sediment. Uplift and erosion at a later time then strips the sedimentary cover, exposing the pluton to Earth's surface. These basement rocks then reside at the surface until deposition of Phanerozoic strata to form the GU that is visible today.

Scenario two is the compound unconformity model. In this hypothesis the initial stages of the GU are similar to the simple unconformity model. The pluton crystallizes within the Precambrian basement, and is overlain by Precambrian sediment. These sediments are then

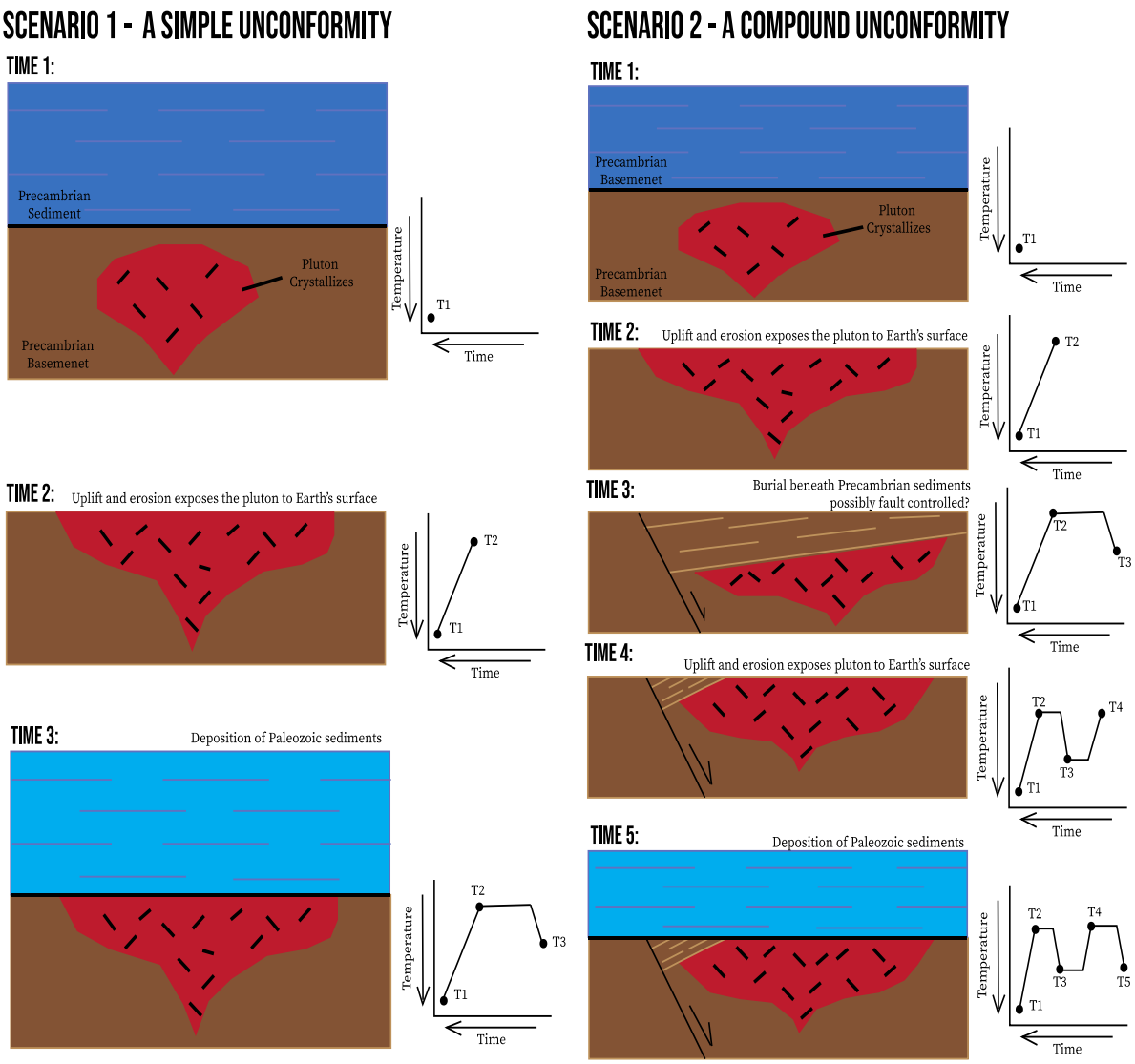

Figure 1: Time series description of the two hypotheses being tested that may have led to the formation of the Great Unconformity. Scenario one is the simple unconformity model while scenario two is the compound unconformity model. Alongside each time series box is an accompanying time-temperature graph that predicts what the thermal history models would be for each scenario.

eroded away, exposing the pluton to the surface. This period of exhumation is then followed by another pulse of Precambrian sedimentation that is possibly fault controlled that reburies the rocks. For this model to be true, a second period of erosion and exhumation must occur to bring these crystalline rocks back to Earth's surface prior to deposition of Paleozoic sediments.

In order to test the compound unconformity hypothesis and to constrain the timing of Precambrian exhumation, a combination of new and existing zircon (U-Th)/He (ZHe) thermochronologic data from five samples is used to construct continuous time-temperature (t-T) paths from ~250 °C to surface temperatures. Samples were collected in New Mexico and Colorado near sites that contain existing $^{40}Ar/^{39}Ar$ data. These results are also interpreted within the context of a compilation of $^{40}Ar/^{39}Ar$ from Colorado and New Mexico, which bear important information on the higher temperature thermal history of this region.

Chapter 2: Background

2.1 The Great Unconformity Within The Grand Canyon

Similar to much of the southwestern United States, the Cambrian Tapeats Sandstone overlies the basement unconformity within the Grand Canyon, representing up to 1.3 billion years of missing rock record. However, the Grand Canyon is different from other areas where the GU is visible because of the exceptional exposure of Precambrian rocks that have been exposed by recent incision of the Colorado River (*Karlstrom & Timmons,* 2012).

Previous studies have determined that within the Grand Canyon area the Paleoproterozoic basement rocks were at depths of 25 km at 1.7 Ga, and were then uplifted and exposed to the surface by 1.3 Ga (*Dumond et al*. 2007). At this point low basins began to form, initiating deposition of the Mesoproterozoic Unkar Group of the Grand Canyon Supergroup. This unit is composed predominantly of layered sedimentary rock along with minimal amounts of basaltic sills, dikes, and flows culminating in four distinct sequences of strata, each representing various depositional environments (*Karlstrom & Timmons,* 2012).

The Pre-Unkar Group nonconformity encompasses the entire unroofing of the basement rock that occurred between 1.66 - 1.25 Ga (Fig. 2) (*Timmons et al*. 2005). Thermochronology of monazite crystals show that the basement rocks decompressed from a depth of 25 km to 10 km beginning at 1.7-1.66 Ga, and mica and K-feldspar $^{40}Ar/^{39}Ar$ thermochronology document cooling from 350 -200 °C by 1200 Ma (*Timmons et al.* 2005). Then follows the pre-Shinumo disconformity, which is of an unknown duration. However, the Dox Formation above the disconformity was deposited between 1150-1100 Ma and the Bass Formation below was deposited between 1250-1150 Ma, suggesting the disconformity could be minor or could represent as much as 50 Ma (*Karlstrom & Timmons* 2012).

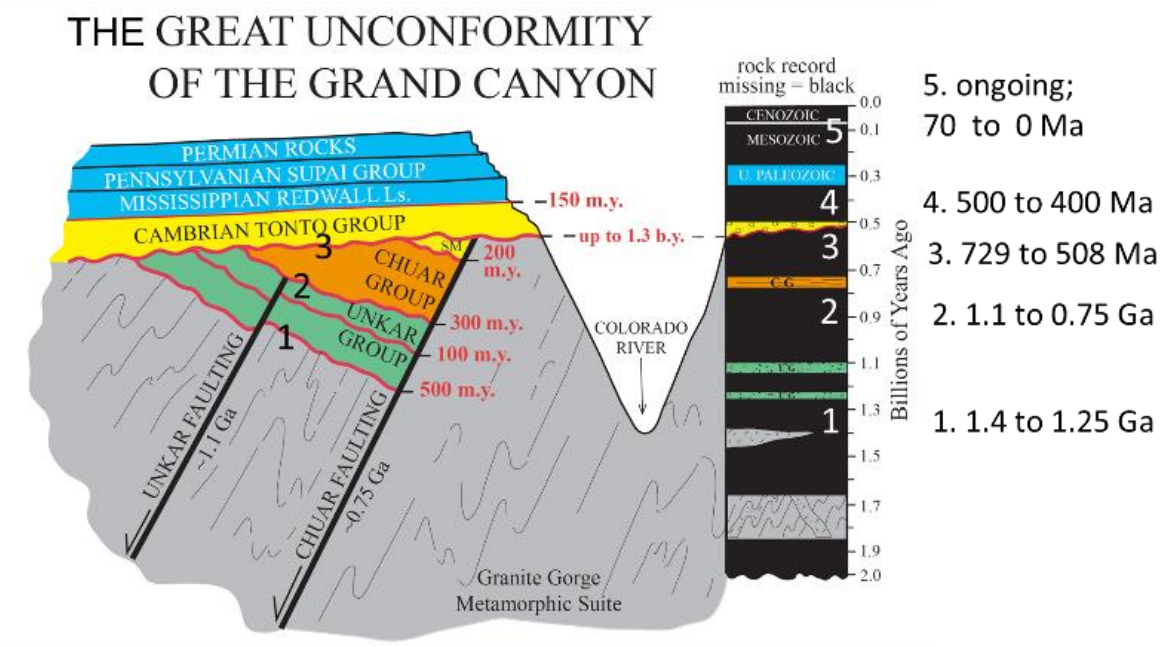

Figure 2. The rock record of the Grand Canyon. Preserved as three major sets: (1) upper horizontal layers of Paleozoic sedimentary strata, (2) titled sedimentary strata of the Grand Canyon Supergroup, and (3) vertically foliated metamorphic and igneous rocks of the Vishnu basement rocks. At right is the time column, with black representing the unconformities (time gaps). The estimated durations of each of the unconformities are labeled in red in millions of years (Ma). SM- Sixtymile Formation; CG – Chuar Group; N – Nankoweap Formation; UG – Unkar Group. Figure is from *Karlstrom et al.* (2019).

The Grand Canyon Supergroup also contains a Neoproterozoic succession, the Chuar Group, which consists of the Galeros and Kwagunt formations (*Karlstrom & Timmons* 2012). The sub-Nankoweap unconformity is now known to represent about 325 m.y., between the 1.1 Ga Cardenas Basalt and the 775 Ma Nankoweap Formation (*Dehler et al*. 2017). Smaller disconformities are possible within both the Unkar and Chuar groups.

The Pre-Nankoweap angular unconformity is also poorly constrained, although new detrital zircon analysis suggest the age of the Nankoweap is <775 Ma, and it is known that the top of the Unkar Group is 1100 Ma (*Karlstrom & Timmons* 2012). Therefore this unconformity could represent as much as 300 Ma. Then follows the Intra-Nankoweap unconformity, which is suggested to have formed during a period of faulting and erosion during Nankoweap deposition (*Karlstrom & Timmons* 2012). This period of erosion is inferred from pebble deposits of Cardenas Basalt within the Nankoweap Formation (*Elston and Scott* 1973). The subsequent Pre-Chuar disconformity is of minimal magnitude, as the Nankoweap Formation is now known to be similar in age and is included into the Chuar Group.

The sub-Sixtymile disconformity is another major unconformity of 200 Ma. The Sixtymile Formation is now known to be <530 Ma, and rests atop the uppermost Chuar Group which is constrained at 729 Ma (*Karlstrom & Timmons* 2012; *Karlstrom et al.* 2018).

Finally, the pre-Tapeats angular unconformity is evident due to the truncation of the Chuar syncline by the horizontal Tapeats Sandstone. The Tapeats Sandstone is a time transgressive formation that is dated at 505 Ma in the western end of the Grand Canyon, and at 501 Ma in the eastern portion (*Karlstrom et al.* 2018). Therefore, due to its placement in relation to the Sixtymile Formation this unconformity could represent up to 140 Ma (*Karlstrom & Timmons* 2012).

The Grand Canyon is one of the few places that exposes such a detailed record of deposition and erosion prior to formation of the GU. At this location, a total of seven individual unconformities are visible within the Grand Canyon Supergroup, suggesting that this embedded set of unconformities in combination creates the Great Unconformity. The exceptional exposure within the Grand Canyon provides strong motivation for investigating the erosional history of Precambrian rocks elsewhere to test the main hypothesis that the GU is a compound surface representing many unconformities.

2.2 PAHRUMP GROUP, DEATH VALLEY, CALIFORNIA

The Pahrump Group in the Death Valley region of eastern California is another prime example of an area that records the missing history of the Precambrian-Cambrian boundary (*Corsetti & Hagadorn* 2000). Recent detrital zircon studies have provided new age constraints for units within the Pahrump Group and can now be precisely correlated with Proterozoic units regionally. Units within the Pahrump Group and the Grand Canyon Supergroup both bear striking similarities in age relations and tectonostratigraphic packages, indicating unconformities observed in both units can be correlated regionally (*Mahon et al.* 2014).

The Pahrump Group rests unconformably on 1700-1400 Ma crystalline basement and includes four formations. From oldest to youngest, these include the lower Crystal Spring Formation, Horse Thief Springs Formation, Beck Spring Dolomite, and the Kingston Peak Formation. Overlying this group is the Noonday Dolomite (*Mahon et al*. 2014).

A major unconformity separates the Crystal Spring Formation and the Horse Thief Springs Formation, and new detrital zircon studies have illuminated the magnitude of this unconformity. Zircon grains analyzed from the Horse Thief Springs Formation sampled directly above the unconformity yielded an average age of 787 ± 11 Ma (*Mahon et al.* 2014). This is roughly 300

million years younger than any of the ages that have been reported from the lower and upper members of the Crystal Spring Formation indicating that the unconformity separating these two formations must at least encompass a gap of 300 Ma (*Mahon et al.* 2014; *Mahon et al.* 2014).

This unconformity can be correlated to the one observed between the Unkar Group-Chuar Group unconformity recognized in the Grand Canyon (Fig. 3) (*Mahon et al.* 2014). Not only do the zircon grains analyzed from these units display similar ages, but the units from the Pahrump group and Grand Canyon group share similar stratigraphies as well. Both the Crystal Spring Formation and the Unkar Group rest above 1700-1400 Ma crystalline basement, are mixed siliciclastic-carbonate units, and contain intrusions by mafic bodies (*Mahon et al.* 2014). The Horse Thief Springs Formation, Beck Spring Dolomite, and Kingston Peak Formation are all correlated with the Chuar Group of the Grand Canyon as well (Fig. 3) (*Mahon et al.* 2014).

The Pahrump Group in Death Valley, California is another prime example of a detailed recording of the deposition and erosion that occurred prior to the formation of the GU. The unconformity between the Crystal Springs Formation and the Horse Thief Springs Formation can be directly correlated to the one observed between the Unkar and Chuar Group in the Grand Canyon, and the stratigraphies of both locations bear striking resemblances to one another.

2.3 Additional Proterozoic Sedimentary Deposits

Additional evidence supporting the compound unconformity model is that there are still some Proterozoic sedimentary deposits exposed within and around New Mexico today. At these localities, Proterozoic sedimentary deposits overlie older crystalline rocks, and are themselves overlain by younger Paleozoic strata. The locations of these deposits are scattered within the area, but their existence raises the possibility that they may have originally covered a greater extent.

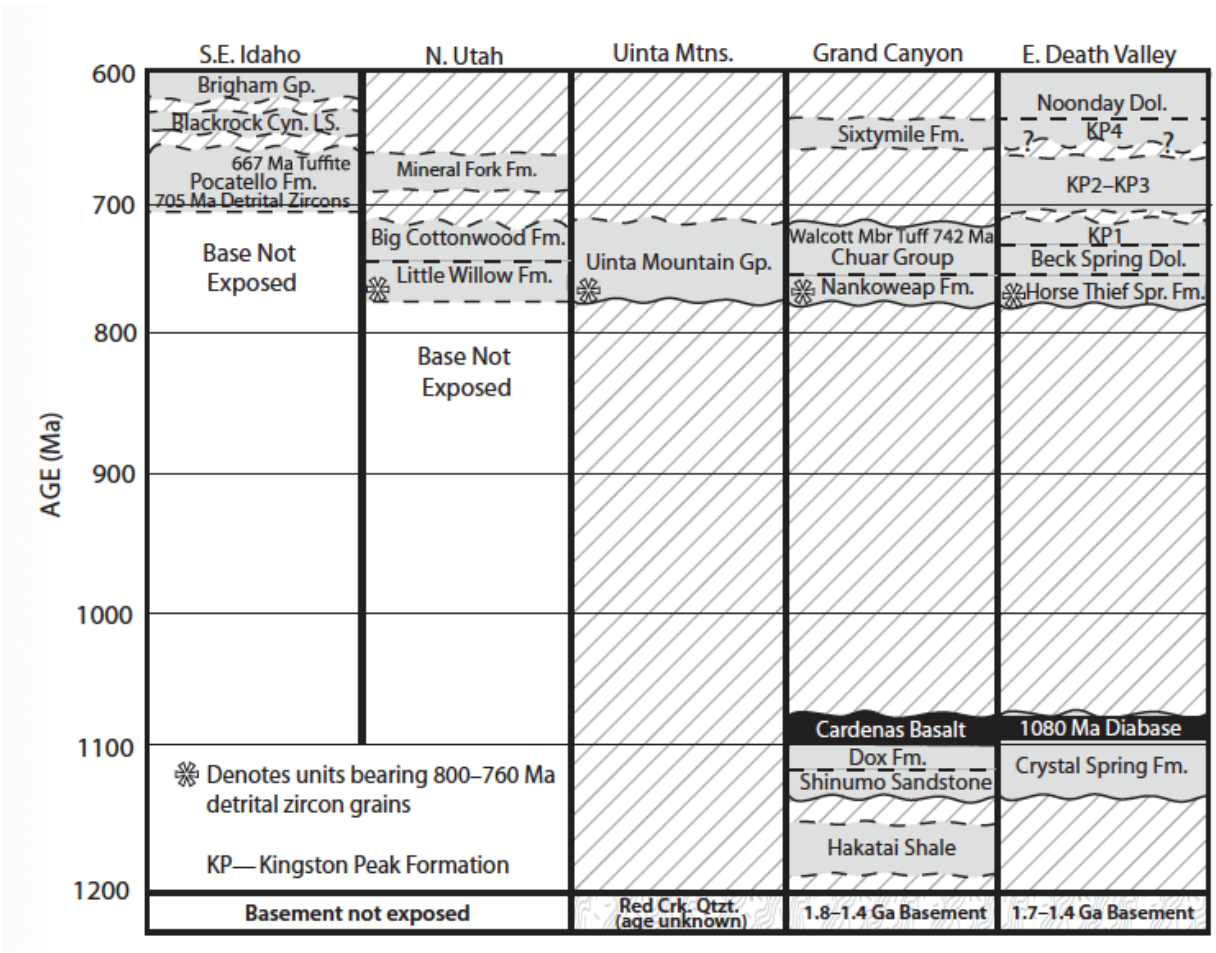

Figure 3: Updated correlation of Mesoproterozoic and Neoproterozoic sedimentary successions in southwestern Laurentia. Bold white asterisk indicates units containing 800-760 Ma detrital zircon grains. Cyn–Canyon; LS-Limestone; Red Crk. Qtzt-Red Creek Quartzite; Mbr-Member; Dol.-Dolomite; Spr.-Springs [*Mahon et al.* 2014].

The Apache Group is one of these Proterozoic sedimentary deposits that is exposed within central Arizona and is also one of the few that can be correlated to members of the Unkar Group in the Grand Canyon (Fig. 4). It has been suggested that the Mescal Limestone of the Apache Group correlates to the Bass Limestone of the Unkar Group (*Shride* 1967*)*. Additionally, the Shinumo Sandstone of the Unkar Group contains similar features as to the Troy Quartzite of the Apache Group (*Shride* 1967). The lower part of the Apache Group contains the Pioneer Shale, which has been dated at 1328 ± 5 Ma, making this lower part of the group too old to correlate with any member of the Unkar Group rocks (*Stewart et al.* 2001). The erosional activity associated with the GU is the only geologic feature that can be correlated with the lower Apache Group, and it is postulated that the material eroded away from the Grand Canyon area during the exhumation period was deposited as part of the lower Apache Group (*Timmons et al.* 2012).

The Hazel Formation, exposed in west Texas, is composed of an orogenic clastic succession including immature boulder conglomerate and sandstone (*Soegaard & Callahan* 1994). Based on the composition of the Hazel Formation and new detrital data from the younger Unkar Group, the 1140-1104 Ma Dox Formation is correlative with the Hazel Formation. The younger deposits of the Hazel Formation record the onset of large-scale mountain building as carbonate deposition came to a halt in this area (*Timmons et al.* 2012).

There are also exposures of Proterozoic sedimentary and volcanic units within the Franklin Mountains in west Texas (*Thomann* 1981). From oldest to youngest, the Precambrian succession is composed of the Castner Marble, the Mundy Breccia, the Lanoria Quartzite, and the Thunderbird Group (*Thomann* 1981). The Castner Marble contains an ash layer that yielded a zircon U-Pb age of 1260 ± 20 Ma (Pittenger et al. 1994). The relationship between limestone

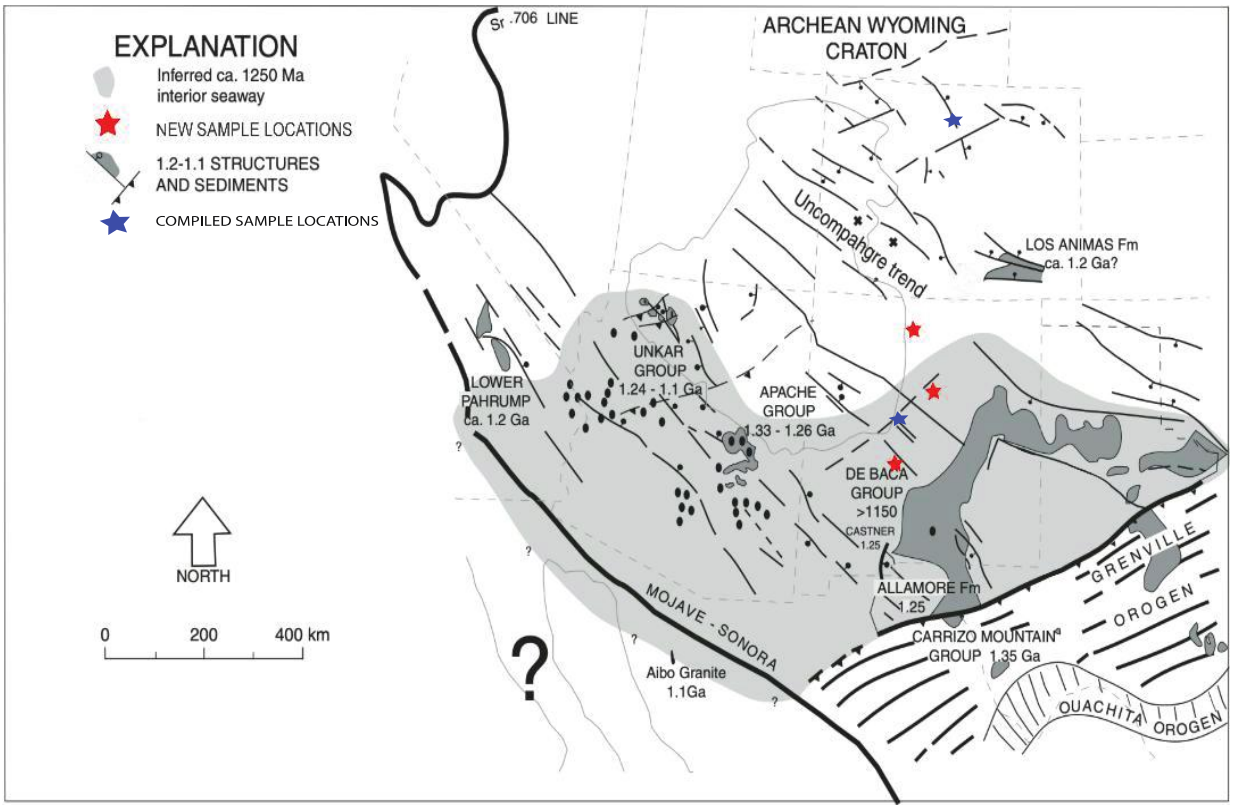

Figure 4: Map showing the 1.25-1.1 Ga sedimentary basins (gray), and tectonic elements associated with the assembly of Rodinia and inboard stresses related to the Greenville convergence. Light gray area represents the hypothesized area of inferred intracratonic seaway at ca. 1250 Ma. Red stars are representative of the locations where new samples were collected for this study. Blue stars are representative of the locations where compiled data was collected for this study. All ages are in billions of years. Map modified from Timmons et al. (2005).

and igneous activity recorded within these units is also similar to what has been seen in the Apache Group in Arizona (*Harbour* 1960).

Additionally, the De Baca Group is exposed in New Mexico and the Las Animas Formation is located in Colorado (Fig. 4) (*Timmons et al.* 2012). Both are believed to be approximately the same age as the Unkar Group, indicating that these Proterozoic sedimentary basins located in the southwestern United States are a key piece of evidence in illuminating the cryptic history of the formation of the GU.

Overall, the existence of these Proterozoic sedimentary deposits and similarities in the timing of deposition raises the possibility that they originally covered a much larger spatial extent. The correlation between many of these deposits to members of the Grand Canyon Supergroup also strengthens the argument that the geologic interpretations gathered from the Grand Canyon area are not an isolated occurrence and can be applied on a much larger scale. The existence of these deposits provides strong motivation to test the hypothesis that the GU exposed in New Mexico and Colorado is a compound unconformity.

2.4 Previous ZHe Thermochronology Studies

There are multiple published studies that utilize ZHe to focus on the formation of the GU, although most of the samples collected for these investigations are outside the intended study area. There are few studies that have focused their sample collection within New Mexico and Colorado that provide new insight into the exhumation history of the GU (*Ault et al*. 2018; *Read* 2019; *Biddle et al.* 2018).

Ault et al. (2018) collected samples from the Sandia Mountains, New Mexico and the Boulder Creek granodiorite in the Front Range, Colorado, and analyzed 14 individual zircon crystals from these sites. Overall the results from both localities demonstrated a negative ZHe

date-eU trend. The ZHe dates from the Sandia Mountains ranged from 555 ± 17 Ma to 19.5 ± 0.6 Ma, and the Boulder Creek samples yielded dates that range from 122 ± 2 Ma to 31.5 ± 0.4 Ma (*Ault et al.* 2018).

The time-Temperature (t-T) forward models for the Sandia sample suggest rapid cooling starting at 1400 Ma, and then a period of residence at near-surface conditions until the Neoproterozoic. The sample was then reburied and exhumed during the Paleozoic and Cenozoic. The Boulder Creek sample experienced a similar history, although the initial cooling period was prolonged such that the duration at near-surface temperatures was much shorter (*Ault et al.* 2018).

Read (2019) compiled 66 zircon (U-Th)/He dates from the Carrizo Mountains, Cookes Range, and Franklin Mountains within west Texas and southern New Mexico. The ZHe dates ranged from 6-731 Ma for the Carrizo Mountains, 44-446 Ma in the Cookes Range, and 19-649 Ma in the Franklin Mountains (*Read* 2019). Both forward and inverse models were created utilizing the collected data and were able to successfully constrain the long-term thermal history of the samples. For the Carrizo Mountains the inverse models implied that a pulse of cooling occurred between ~1100-1000 Ma, and for the Franklin Mountains the models documented a period of Precambrian burial and uplift (*Read* 2019). Inverse modeling for the Cookes Range showed that the majority of cooling for the sample overlaps with the breakup of supercontinent Rodinia (*Read* 2019).

Finally, *Biddle* (2017) collected ZHe dates from southern New Mexico within the Little Hatchet Mountains, Cookes Range, and Franklin Mountains. The ZHe dates ranged from 648.99 ± 89.06 to 19.19 ± 2.46 for all the samples. Additionally, the ZHe dates displayed a distinct grouping when comparing samples collected within the Rio Grande rift and Basin and Range

Province. For example, the ZHe dates from the Rio Grande rift varied from 649-19 Ma, while the ZHe dates from the Basin and Range Province were constrained between 31-21 Ma. This possibly indicates that slightly different extensional magnitudes or processes within the rift compared to the Basin and Range Province (*Biddle,* 2017; *Biddle et al.,* 2018).

Chapter 3: Methodology

3.1 Summary

Previous ZHe and $^{40}Ar/^{39}Ar$ data within New Mexico, Colorado, and Texas have been compiled in order to provide a robust database from which new samples can be compared to. The existing ZHe data are located within central and southern New Mexico and north central Colorado (*Biddle,* 2017; *Biddle et al*., 2018; *Ault et al.* 2018;) (Fig. 5). Additionally, samples from Cookes Range, Franklin Mountains, and the Carrizo Mountains were compiled as well (*Reade* 2019). In order to add to the current ZHe and $^{40}Ar/^{39}Ar$ data three new samples have been collected. One of the samples was collected from Santa Fe, New Mexico. The remaining two samples were collected from Tres Piedras in northern New Mexico and the Los Pinos Mountains in central New Mexico (Fig. 6). All samples consist of Precambrian granitic rocks that lie directly below the GU.

3.2 ZHe Thermochronologic Method

Zircon (U-Th)/He (ZHe) thermochronology involves measuring the total accumulation of ^{4}He produced by the decay of the parent isotopes ^{238}U, ^{235}U, ^{232}Th, and ^{147}Sm. The total concentration is calculated using a two-step analytical procedure. First the crystal is degassed by heating and gas-source mass spectrometry to measure ^{4}He. Then inductively coupled plasma mass spectrometry is utilized on the same crystal to measure U and Th (*Reiners* 2005). The rate at which radiogenic ^{4}He diffuses out of the mineral is dependent upon the temperature and the He diffusivity of the specified mineral (*Reiners & Brandon* 2006). Therefore, once the amount of ^{4}He and parent isotopes is determined this can be used to calculate a He cooling age.

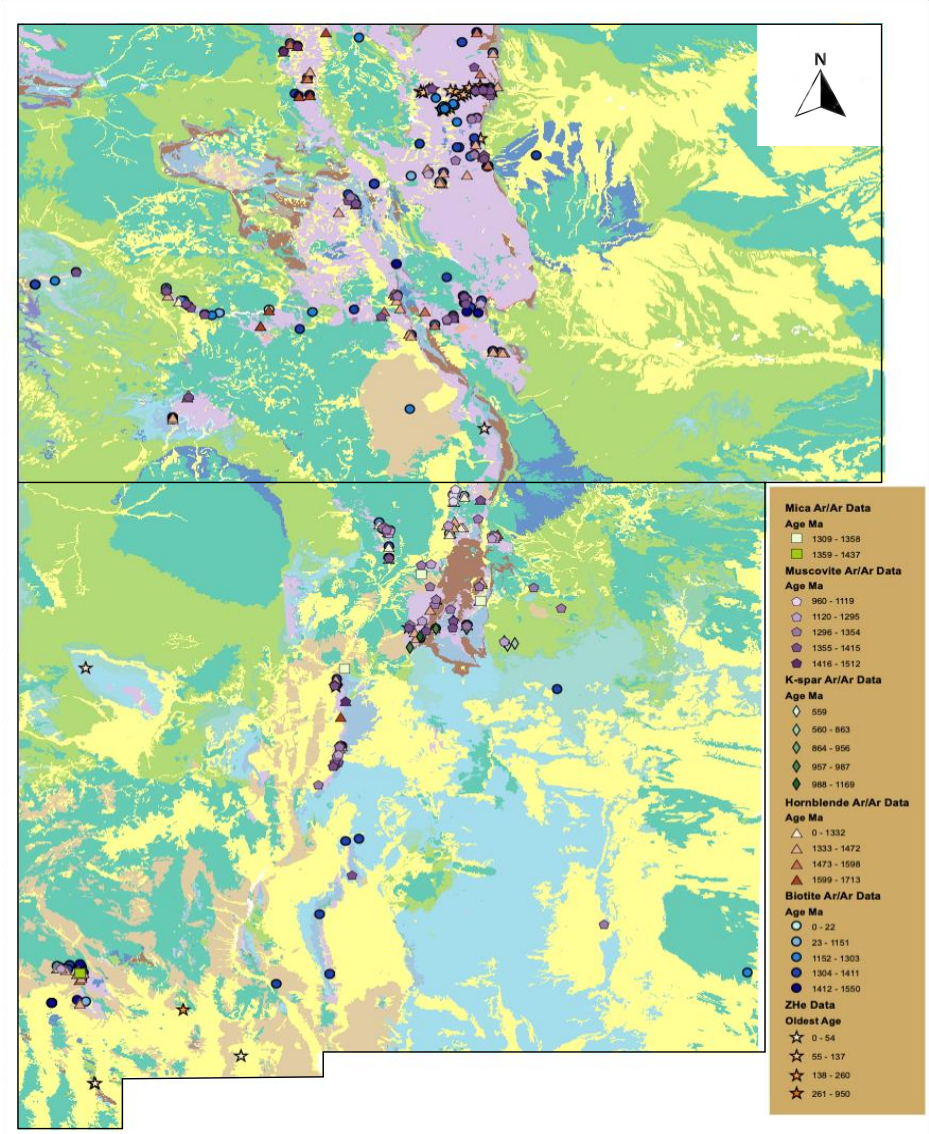

Figure 5: Geologic map of New Mexico and Colorado showing the compilation of ZHe data and $^{40}Ar/^{39}Ar$ data. ZHe data points are represented by the oldest age date for that sample site. [Shaw et al. (2005); Alrdich et al. (1958); Giffin and Kulp, 1960; Goldich et al. (1966); Hansen and Peterman (1968); Marvin and Dobson (1979); Muehlberger et al. (1966); Peterman et al. (1968); Rice et al. (1982); Shaw et al. (1999); Abitz et al. (1987); Aldrich et al. (1957); Alrdich et al. (1958); Brookins and Shafiqullah (1975); Brookins et al. (1975); Brown et al. (1999); Grambling and Dallmeyer (1993); Gresens (1975); Hedlund (1978a); Hedlund (1978b); Hedlund (1980); Karlstrom et al. (1997); Kirby et al. (1995); Marcoline et al. (1999); Muehlberger and Denison (1964); Muehlberger et al. (1966); Pedrick (1995); Marcoline et al. (1995); Thompson et al. (1991); Thompson et al. (1996); WoldeGabriel (1990); Sanders et al. (2006); Erslev et al. (2004); Amato et al. (2011); Ault et al. (2018); Biddle (2017); Johnson et al. (2015); Ault et al. (2018)]

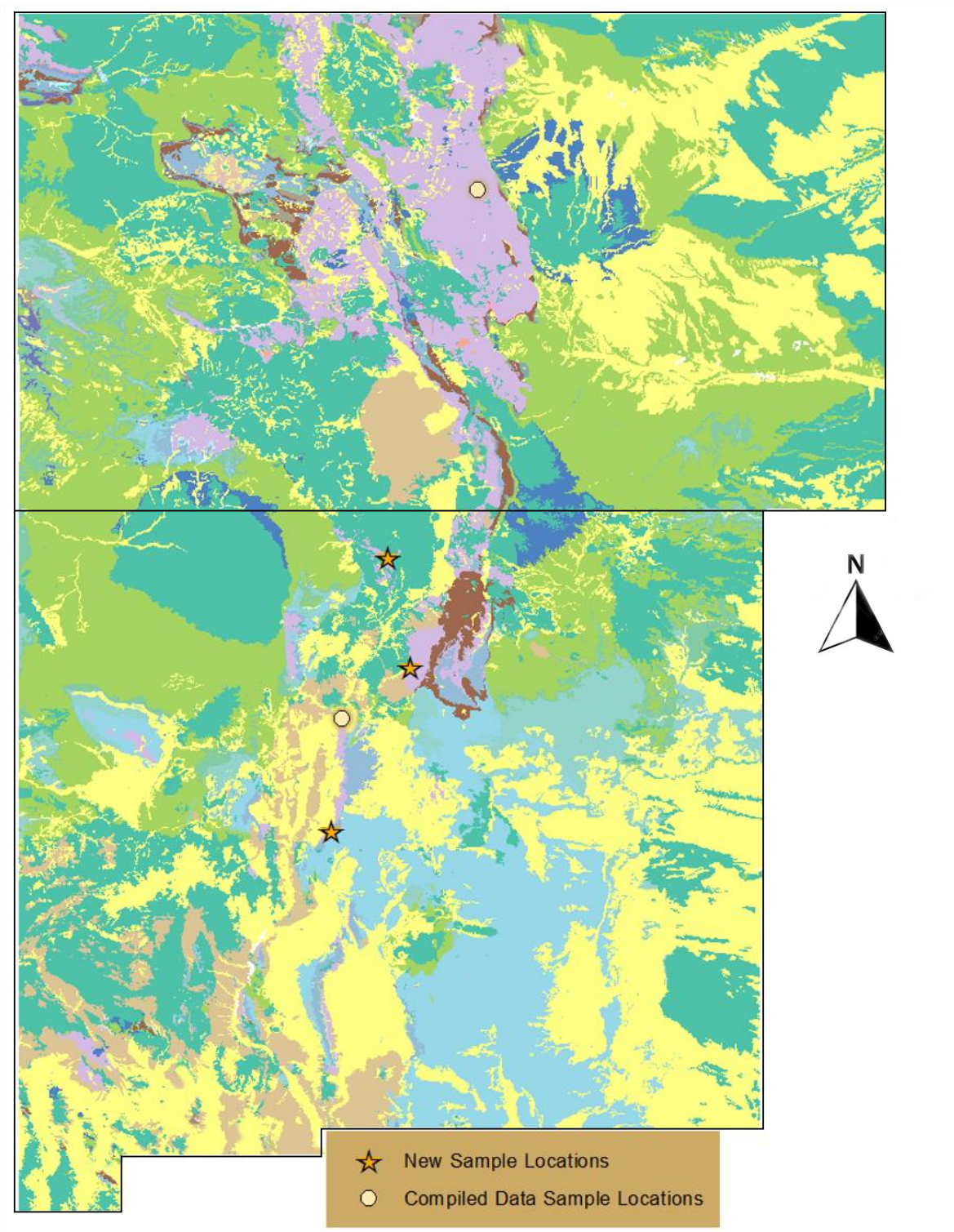

Figure 6: Geologic map of New Mexico and Colorado showing the locations where samples were collected. Stars designate newly collected sample locations. Circles represent previously collected data from other sources.

In this dating method, the mineral being analyzed will reach a point where they no longer lose ^{4}He due to cooling to a low enough temperature, which is known as the closure temperature (*Reiners 2005*). However, prior to reaching this critical temperature there is a range of temperatures that minerals can partially retain He known as the partial retention zone (PRZ) (*Reiners & Brandon* 2006). For the ZHe dating method the PRZ can reach a value as high as 250 °C, and recent estimates place the lower limit of the PRZ at ~50°C (*Guenthner et al.*, 2013; *Johnson et al*. 2015). Utilizing a geothermal gradient of 25 °C/km and a surface temperature of 15 °C this corresponds to depths of ~1.5-9.5 km making this method useful for studies involving upper crustal to near surface processes (*Reiners* 2005; *Reiners & Ehlers* 2018).

The effective uranium concentration (eU; [U] + 0.235 [Th]) is representative of the α productivity for the decay of U and Th concentrations (Flowers et al., 2009). In zircon grains the eU concentration can greatly affect the accumulation of radiation damage, which will lead to fluctuations in He diffusivities (*Guenthner et al*. 2013). If the radiation damage is less than 1.5 x 10^{18} α/g the effective diffusivity of the grain is found to decrease. This decrease can be attributed to increasing disruption of diffusion fast-paths such as the c-axis parallel channels resulting in He being restricted to the less favorable c-axis orthogonal apertures (*Guenthner et al*. 2013). The end result is a positive trend between ZHe dates and eU, indicating a slow cooling period through the ZHe PRZ. Conversely, if radiation damage is above 1.5 x 10^{18} α/g then the He diffusivity is found to rapidly increase. Damaged zones within the grain become interconnected, and lead to rapid diffusion pathways for He to become available leading to surge in diffusivity. Ultimately, this would result in a negative correlation between ZHe dates and eU concentration if the sample resides within the PRZ for prolonged periods of time (*Guenthner et al.* 2013). Individual zircon crystals from a single sample typically have a range of eU values and related

ZHe dates. A spread in ZHe dates with either positive or negative relationships with eU values is necessary to investigate the thermal history of the sample.

3.3 ^{40}Ar/^{39}Ar Thermochronologic Method

Similar to ZHe thermochronology the Ar dating method utilizes a noble gas, and is controlled by thermally activated diffusion. The Ar dating method is based off the decay of ^{40}K to radiogenic ^{40}Ar (*Reiners & Brandon* 2006). Argon diffusion in common rock-forming minerals is sensitive to higher temperatures than He diffusion in zircon, so Ar cooling ages are typically older than He cooling ages. Gas source mass spectrometry is used to calculate the Ar ages, and involves converting a portion of ^{39}K to ^{39}Ar by neutron irradiation before degassing takes place. From this point the initial amount of the parent ^{40}K can be determined by utilizing the production rate of ^{39}Ar during the neutron irradiation and the ^{40}K/^{39}K ratio (*Reiners & Brandon* 2006). Finally, the Ar cooling age is calculated using the ^{40}Ar/^{39}Ar ratio.

As with the ZHe dating method the minerals used to calculate Ar dates are also sensitive to certain temperatures, and are associated with unique boundaries where they are able to partially retain the radioisotopic decay product. The four minerals that are commonly used to obtain Ar dates are hornblende, muscovite, biotite, and K-feldspar. Each mineral is associated with a unique PRZ, and the width of each PRZ is found to increase as temperatures increase (*Reiners & Brandon* 2006). Hornblende has the largest PRZ ranging from 575-425 °C (Fig. 7). Muscovite has an upper limit of 400 °C, and partially retains ^{40}Ar until 250 °C. Biotite has a PRZ range from 350 °C to 250 °C. Finally, K-feldspar has the lowest PRZ with an upper limit of 225 °C, and a lower extent of 125 °C (Fig. 7) (*Reiners & Brandon* 2006).

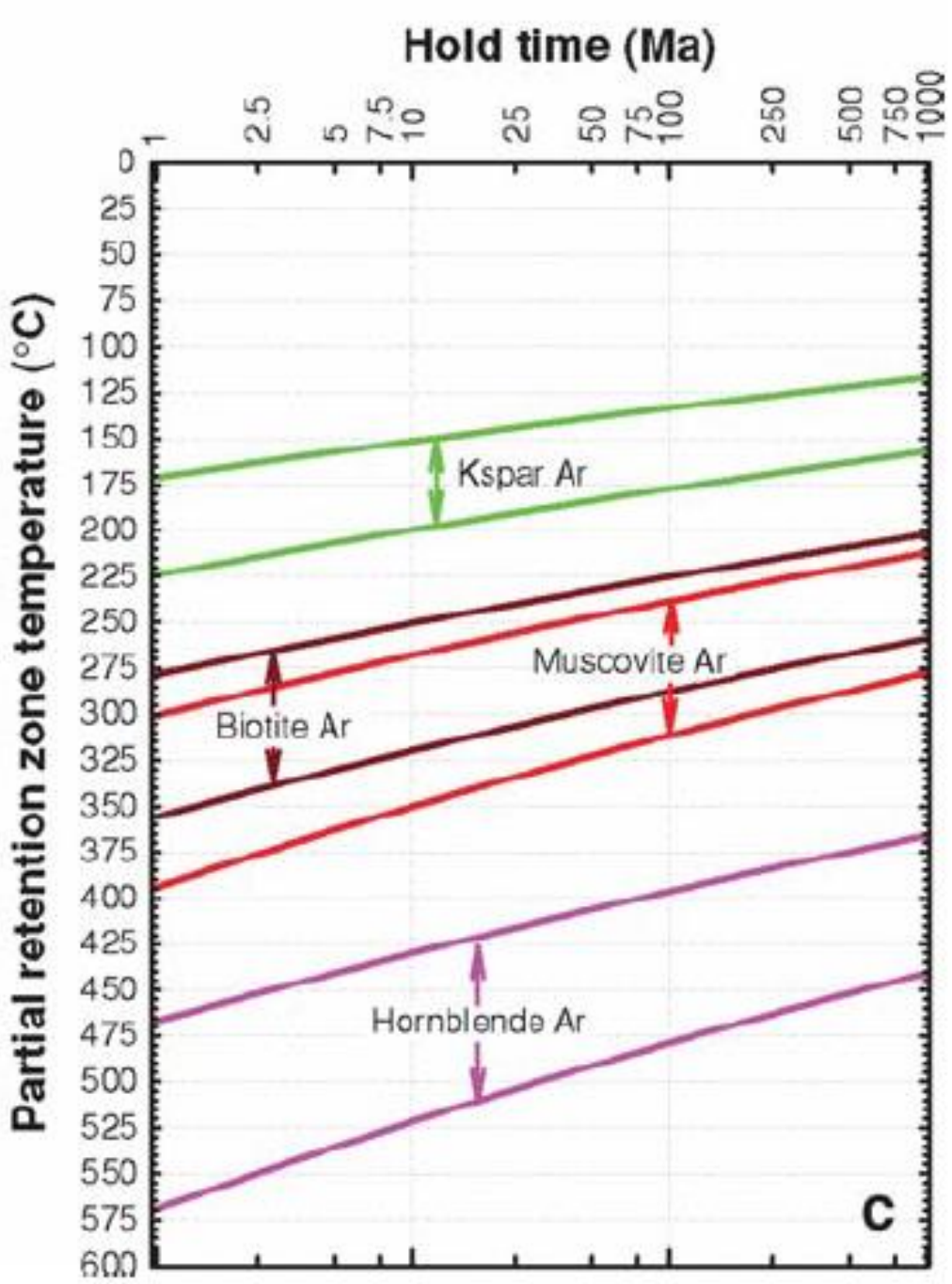

Figure 7: Partial retention zones (PRZs) for Ar thermochronometers. The PRZ for each thermochronometer is defined by upper and lower boundaries, which corresponds to 90% and 10% retention respectively after being retained at a steady temperature for a specific amount of time. Figure is from *Reiners & Brandon* (2006).

3.4 Mineral Separation

Sample processing involved standard rock crushing mineral separation techniques. The first step in this process is crushing the rocks using a Braun Chipmunk Jaw Crusher. The crushed rocks are then further reduced in size utilizing a Bico UA Pulverizer. Once this process is complete the pulverized samples are then sieved and panned in water to separate and collect dense minerals. Magnetic minerals were sorted out by first utilizing a hand magnet, and then a Frantz Magnetic Separator. Finally, the remaining material was processed using a heavy liquid separation process where the individual zircon crystals were collected for further analysis.

Individual zircon crystals were hand selected under a microscope for analysis. Suitable crystals must be euhedral, inclusion-free, and have a minimum width of 70 μm. Ideally, a total of ten zircon grains were to be collected from each sample, although in some cases less than ten suitable grains were found. In order to capture the widest range in eU values and ZHe ages, techniques outlined in *Ault et al.* (2018) were used. *Ault et al*. (2018) note a relationship between zircon appearance and eU, where higher eU values correspond to an increase in opacity and discoloration. During mineral selection, zircon grains with a wide range of appearances were selected, from clear and translucent to opaque and discolored, in order to capture a wide range of eU values. The length and widths of each zircon crystal were measured in order to apply an Ft age correction (*Farley et al.* 1996). These grains were then packaged in Nb tubes before being sent to the (U-Th)/He Thermochronology Lab at CU Boulder for analysis.

3.5 Thermal History Modeling

New and compiled thermochronologic data were analyzed using HeFTy software (*Ketcham* 2005). This program allows a user to relate thermochronologic data to possible t-T histories. There are two main ways this program is currently utilized. In a forward model, the

user can specify a hypothetical t-T path, and HeFTy can be used to calculate the predicted zircon age-eU relationship using the diffusion parameters of *Guenthner et al*. (2013). Alternatively, the user can input ZHe information, including age, U and Th concentration, and grain size, to constrain possible t-T paths that yield statistically significant fits to the data. This inverse model approach can be used to narrow down the possible thermal histories that are permitted by the data. Both forward and inverse modeling approaches were used in this study in order to document the timing of formation of the GU and test the hypothesis that these Precambrian rocks experienced multiple burial and uplift events prior to deposition of Paleozoic strata.

Forward Modeling

For this method predetermined time-temperature paths were input into the HeFTy software in order to calculate the corresponding thermochronometric age from each specific path. The resulting ZHe date-eU curves can then be compared to collected ZHe data in order to determine whether that path is viable for each sample (*Guenthner et al.* 2013). This method was utilized to constrain possible time-temperature paths for the three newly collected samples from Tres Piedras, Santa Fe, and Los Pinos Mountains. For each sample all available geologic constraints were applied in order to construct hypothetical t-T paths (Table 1). For each sample, twelve hypothetical time-temperature paths were tested in order to try and constrain the thermal history for each sample.

Inverse Modeling

Inverse modeling calculates time-temperature paths that correspond to measured thermochronometric ages within a certain error percentage. HeFTy utilizes a Monte Carlo

Table 1: Thermal history model input table for forward and inverse simulation of zircon (U-Th)/He data from Los Pinos, Tres Piedras, Santa Fe, Sandia Mountains, and Front Range.

1. Thermochronologic data

Samples and data used in inverse simulations

Los Pinos, Tres Piedras, Santa Fe, Sandia Mountains, and Front Range

ZHe data

Data treatment, uncertainties, and other relevant constraints

Los Pinos

Treatment: ZHe data were binned based on observed clusters of ZHe data that plot in similar locations for sample 89LP08

	ZHe Date (Ma)	Error (Ma)	Error (%)	eU (ppm)	Bins
Synthetic grain 1	676	101	15%	126	Average of grains z5 and z6
Synthetic grain 2	664	100	15%	169	Average of grains z14 and z09
Synthetic grain 3	304	46	15%	297	Average of grains z10, z1, z16, z11, z3, and z2
Synthetic grain 4	170	26	15%	397	Average of grains z13 and z08
Synthetic grain 5	163	24	15%	537	Equal to grain z4
Synthetic grain 6	97	14	15%	708	Average of grains z07 and z12

Tres Piedras

Treatment: ZHe data were binned based on observed clusters of ZHe data that plot in similar locations for sample 18TUS03

	ZHe Date (Ma)	Error (Ma)	Error (%)	eU (ppm)	Bins
Synthetic grain 1	303	45	15%	344	Average of grains z07, z17, and z08
Synthetic grain 2	354	53	15%	444	Average of grains z01, and z03
Synthetic grain 3	226	34	15%	527	Average of grains z10, z06, and z12
Synthetic grain 4	177	27	15%	656	Average of grains z15, z09, and z11
Synthetic grain 5	47	7	15%	1379	Equal to grain z05
Synthetic grain 6	50	8	15%	1477	Equal to grain z04

ZHe dates (Ma):

r (um): Mean equivalent spherical radius of each bin

eU (ppm): Mean eU of each bin

Error (Ma) applied in modeling: Input errors are a certain percent of the corrected age of each synthetic grain. 15% error was initially used for each grain, and yielded good paths for each sample.

2. Additional geologic information

These constraints are also plotted visually on the inverse model results

Santa Fe, NM

Assumption	Explanation and data source
> 300 °C at ~ 1700 Ma	Crystallization age by U-Pb zircon geochronology (Karlstrom 2004).
*25-5 °C between 1600-1500 Ma	*Constraint box to allow for rapid exhumation after crystallization and test for burial during the Precambrian time period
*300-50 °C between 1500-360 Ma	*Large constraint box to allow for burial prior to the formation of the Great Unconformity
25-5 °C between 360-320 Ma	Paleozoic (Mississippian) deposition on Precambrian units (Read et al. 2000).
300-40 °C between 320-20 Ma	Large constraint box allows for burial prior to oldest apatite fission track ages that record temperatures of 120 °C at 50 Ma (Kelley et al. 1992).
35-25 °C between 12-7 Ma	Based on apatite fission track ages (Kelley et al. 1992).

Tres Piedras, NM	
Assumption	**Explanation and data source**
> 300 °C at ~1650 Ma	Crystallization age based on U-Pb zircon geochronlogy (Wobus 1984).
*25-5 °C between 1590-1530 Ma	*Constraint box to allow for rapid exhumation after crystallization and test for burial during the Precambrian time period
300-10 °C between 1530-560 Ma	*Large constraint box to allow for burial prior to the formation of the Great Unconformity
25-5 °C between 560-470 Ma	Cambrian Bill Formation unconformably lies on top of Precambrian granite (Amato & Mack 2012).
300-40 °C between 280-80 Ma	Burial prior to the potential Laramide/Rio Grande rift uplift (Cather 2004).
Los Pinos, NM	
Assumption	**Explanation and data source**
>300 °C at ~1660 Ma	U-Pb geochronology of zircons indicate approximately the same age for all three Precambrian units (Shastri & Bowring 1992).
*45-10 °C between 1600-1500 Ma	*Constraint box to allow for rapid exhumation after crystallization and test for burial during the Precambrian time period
*300-35 °C between 1500-320 Ma	*Large constraint box to allow for burial prior to the formation of the Great Unconformity
35-5 °C between 320-280 Ma	Pennsylvanian strata lay with an angular unconformity on the Precambrian rocks (Johnson & Read 1952).
300-40 °C between 280-80 Ma	Burial prior to the potential Laramide/Rio Grande rift uplift (Cather 2004).
130-25 °C between 70-30 Ma	Based on apatite fission track ages (Kelley et al. 1992).
Sandia Mountains, NM	
Assumption	**Explanation and data source**
> 300 °C at ~ 1400 Ma	Crystallization age by U-Pb zircon geochronology (Kirby et al. 1995).
*40-5 °C between 1320-1270 Ma	*Constraint box to allow for rapid exhumation after crystallization and test for burial during the Precambrian time period
*300-5 °C between 1270-570 Ma	*Large constraint box to allow for burial prior to the formation of the Great Unconformity
35-5 °C between 570-530 Ma	Precambrian-Mississippian regional unconformity places basement exposures at or near the surface
120-80 °C between 430-360 Ma	Limited Early Paleozoic reburial (Kelley and Northrup. 1975).
60-5 °C between 330-260 Ma	Pennsylvanian San Andres and Madera Formations unconformably overlie Sandia granite in Sandia Mountains
180-150 °C between 45-10 Ma	Consistent with apatite He date-eU patterns and thermal history simulations of AFT and apatite He dates from Sandia granite (House et al. 2003; Ricketts et al. 2015).

Front Range, CO

Assumption	Explanation and data source
> 300 °C at ~ 1700 Ma	Crystallization age by U-Pb zircon geochronology (Premo and Fanning 2000).
320-280 °C between 1330-1280 Ma	Based on Ar/Ar biotite thermochronlogy (Shaw et al. 1999).
*30-5 °C between 1280-1200 Ma	*Constraint box to allow for rapid exhumation after crystallization and test for burial during the Precambrian time period
*300-20 °C between 1200-600 Ma	*Large constraint box to allow for burial prior to the formation of the Great Unconformity
20-5 °C between 600-550 Ma	Early Paleozoic sedimentary rocks unconformably overlie Precambrian basement
300-20 °C between 540-320 Ma	Early Paleozoic sedimentary rocks unconformably overlie Precambrian basement
25-5 °C between 320-260 Ma	Penn-Perm Fountain Formation unconformably ovelries Boulder Creek granodiorite at mouth of Boulder Canyon
180-140 °C between 70-35 Ma	62 Ma AFT data from Boulder Creek granodiorite near Boulder Canyon (Kelley and Chapin 1994).

**: Denotes constraint boxes that were used only in the reburial inverse model scenarios*

3. System- and model-specific parameters

He kinetic model: ZRDAAM (Guenthner et al., 2013) for all ZHe data
Statistical fitting criteria: "Good" fits are defined as those for which the mean of the GOF statistics assessed is 0.5, and the minimum is 1/(N+1), where N is the number of statistics used (Ketcham et al., 2009).
Modeling code : HeFTy v1.9.3
Number of tT paths attempted: 50,000 -100,000
tT path characteristics: Monotonic consistent, Halve 5 times, Episodic

method to create various plausible time-temperature paths based on the grain data entered (*Ketcham* 2005). A maximum of seven grains can be entered into the program and the input information includes U and Th concentration, grain radius, measured age, and a percentage of uncertainty. For this study a 15% error was utilized for all grains. Additionally, if more than seven grains are available for a specific sample, then "synthetic grains" must be created. In this study synthetic grains were created for the Tres Piedras and Los Pinos Mountains samples. For both samples the ZHe dates were binned according to their eU content in intervals of 100 ppm (Table 1).

Once the grain information is input, all available geologic constraints are then applied according to any known periods of burial or exhumation. These constraints are represented by boxes in the inverse model and the paths are forced to go through these rectangles. The same geologic constraints utilized for the forward modeling were used in inverse modeling (Table 1). Finally, HeFTy then constructs a certain number of paths according to the number entered by the user. For this project a total of 50,000-100,000 paths were run for each sample. HeFTy then separates paths into two groups based of goodness-of-fit parameters. "Acceptable" paths have goodness-of-fit parameters >0.05 and "good" paths have goodness-of-fit parameters of >0.5. The resulting paths that fall within one of these two categories will then be recorded on one time-temperature plot.

Inverse modeling was utilized to examine all the new and compiled ZHe data from New Mexico and Colorado. In total, five samples were tested with this method, including the Sandia Mountains, Boulder Creek, Los Pinos Mountains, Tres Piedras, and Santa Fe.

Chapter 4: Results

4.1 Rock Descriptions

All samples collected for analysis consisted of exposed Proterozoic basement starting with the ~1.65 billion-year-old pink foliated granite collected from Santa Fe, NM (Fig. 6) (*Spiegel et al.* 1963). Followed by the Tres Piedras granite, which is a pink, fine to medium grained, foliated quartz monzonite (*Wobus* 1984). The last newly collected sample was the Proterozoic gneiss from the Los Pinos Mountains. The Los Pinos granite is generally described as a phaneritic pink granite that is gneissic in certain areas (Fig. 6) (*Muehlberger & Denison* 1964). The two compiled samples consisted of the Sandia granite of the Sandia Mountains and the Boulder Creek granodiorite of Front Range, CO. The Sandia granite is a grey to pink, medium to coarse grained, phaneritic rock (*Brookins & Majumdar* 1982). The Boulder Creek granodiorite is a gray, fine to medium grained, slightly foliated intrusive rock (*Gable* 1972).

4.2 ZHe Dates

A total of 37 new individual grain ZHe dates were obtained for this project, including nine from Nuns Curve in Santa Fe, NM, 13 from Tres Piedras, NM, and 15 from the Los Pinos Mountains, NM (Fig. 6). Additionally, six ZHe dates from the Sandia Mountains, NM and eight ZHe dates from Front Range, CO collected by *Ault et al.* (2018) were incorporated for analysis. In total, this project uses 51 individual grain ZHe dates from five samples to investigate the timescales and processes associated with formation of the GU in Colorado and New Mexico (Table 2).

Table 2: Zircon (U-Th)/He Data

Table 2: Zircon (U-Th)/He Data

Sample	Mass (µg)	Spherical Radius (µm)	4He (nmol/g)	U (ppm)	Th (ppm)	eU (ppm)	Raw Date (Ma)	Ft	Corrected Date (Ma)	2σ
Santa Fe, NM										
18NC01 : Precambrian granite. 35.724972°N -105.887639°W, Elev. 2321m										
18NC01_z1	3.51	38.70	772.552	191.46	157.08	228.4	595.86	0.710	822.48	43.90
18NC01_z2	6.69	52.94	548.588	606.97	1227.51	895.4	112.46	0.777	144.33	4.47
18NC01_z3	3.37	40.93	612.832	236.26	618.79	381.7	291.08	0.716	403.25	41.40
18NC01_z4	6.21	52.44	342.432	1065.04	1226.41	1353.2	46.71	0.779	59.89	1.44
18NC01_z5	7.17	44.73	477.288	101.92	133.57	133.3	630.32	0.741	835.06	31.94
18NC01_z6	4.23	43.15	0.007	0.38	0.38	0.5	2.76	0.737	3.75	14.44
18NC01_z7	9.45	60.35	0.090	0.48	0.74	0.7	25.49	0.806	31.60	6.53
18NC01_z8	12.01	64.50	535.585	384.77	773.87	566.6	172.75	0.815	211.22	6.20
18NC01_z9	2.31	31.79	0.057	0.75	1.02	1.0	10.68	0.65	16.54	24.48
Los Pinos Mountains, NM										
89LP08 : Proterozoic gneiss. 34.40383°N -106.5265°W, Elev. 1704 m										
89LP08_z1	2.92	42.65	235.202	231.55	162.28	269.7	159.54	0.735	215.99	4.41
89LP08_z12	2.05	38.32	326.642	672.01	312.91	745.5	80.71	0.709	113.51	4.15
89LP08_z2	5.43	48.89	309.311	307.16	179.38	349.3	161.95	0.769	209.71	8.03
89LP08_z3	2.27	39.07	631.377	284.09	150.12	319.4	355.41	0.713	491.90	24.14
89LP08_z4	3.76	48.78	368.403	483.83	226.77	537.1	125.85	0.768	163.28	4.47
89LP08_z5	8.39	59.58	292.972	100.28	53.44	112.8	462.28	0.807	567.05	21.41
89LP08_z6	2.77	40.20	455.768	119.08	87.93	139.7	575.28	0.718	785.28	27.93
89LP08_z07	6.13	54.71	229.484	629.49	170.22	669.5	63.26	0.793	79.62	2.91
89LP08_z08	4.65	51.16	182.925	380.59	161.63	418.6	80.51	0.778	103.18	2.73
89LP08_z09	3.76	48.66	370.114	163.50	91.73	185.1	359.45	0.767	464.27	27.81
89LP08_z10	4.62	47.84	603.207	223.19	125.51	252.7	426.46	0.763	552.59	17.58
89LP08_z11	7.87	60.18	227.937	264.45	133.95	295.9	141.13	0.810	173.78	7.70
89LP08_z13	4.43	49.31	377.971	334.45	172.60	375.0	183.98	0.770	237.77	12.18
89LP08_z14	5.28	48.94	594.178	132.75	88.66	153.6	675.87	0.769	863.86	27.25
89LP08_z16	6.65	55.20	232.275	269.16	104.37	293.7	144.87	0.795	181.50	7.37
Tres Piedras, NM										
18TUS03 : Precambrian granite. 36.616176°N -106.068948°W, Elev. 2501 m										
18TUS03_z01	5.10	49.92	695.854	409.53	140.78	442.6	284.35	0.774	364.73	14.00
18TUS03_z03	10.93	62.94	694.166	408.95	151.28	444.5	282.51	0.818	343.30	11.11
18TUS03_z04	4.41	47.41	306.153	1382.20	403.42	1477.0	38.34	0.763	50.19	1.56
18TUS03_z05	3.32	43.09	262.385	1290.19	376.42	1378.7	35.21	0.743	47.34	2.39
18TUS03_z06	3.44	42.25	499.405	442.39	290.93	510.8	178.58	0.735	241.70	15.56
18TUS03_z07	4.51	46.72	397.004	294.38	101.21	318.2	226.87	0.761	296.30	13.42
18TUS03_z08	5.34	48.20	477.682	340.17	111.32	366.3	236.87	0.767	306.63	10.42
18TUS03_z09	9.75	57.50	380.447	634.03	176.30	675.5	103.56	0.804	128.57	5.72
18TUS03_z10	5.15	51.29	470.027	463.27	174.31	504.2	170.36	0.779	217.63	6.82
18TUS03_z11	2.65	42.30	464.463	627.61	269.64	691.0	123.36	0.735	167.14	8.67
18TUS03_z12	3.53	42.19	502.148	523.67	177.26	565.3	162.45	0.735	219.92	6.92
18TUS03_z15	3.87	46.04	587.947	562.33	172.31	602.8	178.12	0.756	234.38	15.19
18TUS03_z17	2.39	35.99	406.007	319.89	113.33	346.5	213.30	0.694	304.53	23.35
Sandia Mountains, NM										
MC14-s6: Precambrian granite. 35.21113°N -106.47831°W, Elev. 2237 m										
z1	2.10	42	291	195	117	223	237.0	0.71	332.0	20.0
z2	3.00	45	246	152	103	176	253.0	0.73	345.0	20.0
z3	6.30	55	370	130	93	152	435.0	0.78	555.0	34.0
z4	5.70	54	227	82	74	100	408.0	0.77	526.0	32.0
z5	4.70	51	100	326	150	362	51.0	0.76	67.0	4.0
z6	3.20	44	89	1077	416	1175	14.1	0.73	19.5	1.2
Front Range, CO										
A12-8: Precambrian granodiorite. 40.01281°N -105.30953°W, Elev. 1703 m										
z1	5.3	45	199	561	103	586	63.0	0.73	85.0	2.0

z2	2.5	39	159	319	102	342	85.0	0.70	122.0	4.0
z3	3.6	41	199	396	150	431	85.0	0.71	120.0	4.0
z4	4.0	44	212	418	83	437	89.0	0.73	122.0	4.0
z5	8.6	49	216	559	234	614	65.0	0.75	86.0	2.0
z6	3.8	41	106	822	236	878	22.3	0.71	31.5	0.8
z8	7.3	54	196	605	242	662	55.0	0.77	71.0	2.0
z9	6.3	51	175	701	298	771	42.0	0.76	55.2	1.6

Los Pinos Mountains, New Mexico

Fifteen ZHe dates were obtained from one Precambrian granite sample collected below the GU from the Los Pinos Mountains in New Mexico. The ZHe dates obtained from these grains show a large spread, ranging from 79.62 – 863.86 Ma. The eU concentration of these fifteen grains range from 112.8 – 745.5 ppm (Fig. 8). Overall, ZHe dates from this sample show a well-defined negative trend with eU. Additionally, no correlation is observed between the date and recorded radius of the grains (Fig. 8).

Tres Piedras, New Mexico

Thirteen ZHe dates were obtained from one Precambrian granite sample collected directly below the GU from Tres Piedras New Mexico. The ZHe dates obtained from this sample display a moderate spread, ranging from 47.34 – 364.73 Ma (Fig. 8). The eU concentration of these grains did result in large spread, ranging from 318.2 – 1477 ppm. Overall, a negative trend between the ZHe dates and eU is observed and no correlation can be made between the ZHe dates and radius (Fig. 8).

Santa Fe, New Mexico

Nine ZHe dates from one sample were obtained from the Precambrian granite just below the GU at the Nuns Curve outcrop in Santa Fe, NM. Of these nine dates, three have been removed due to anomalously low He, U, and Th (Table 2). This could have possibly been due to the grains falling out of the tube during the packaging process, or if a grain other than zircon was analyzed. The remaining six ZHe dates obtained from this sample show a large spread in ZHe date, ranging from 31.6 – 835.06 Ma. Additionally, the spread in eU also contained a large range

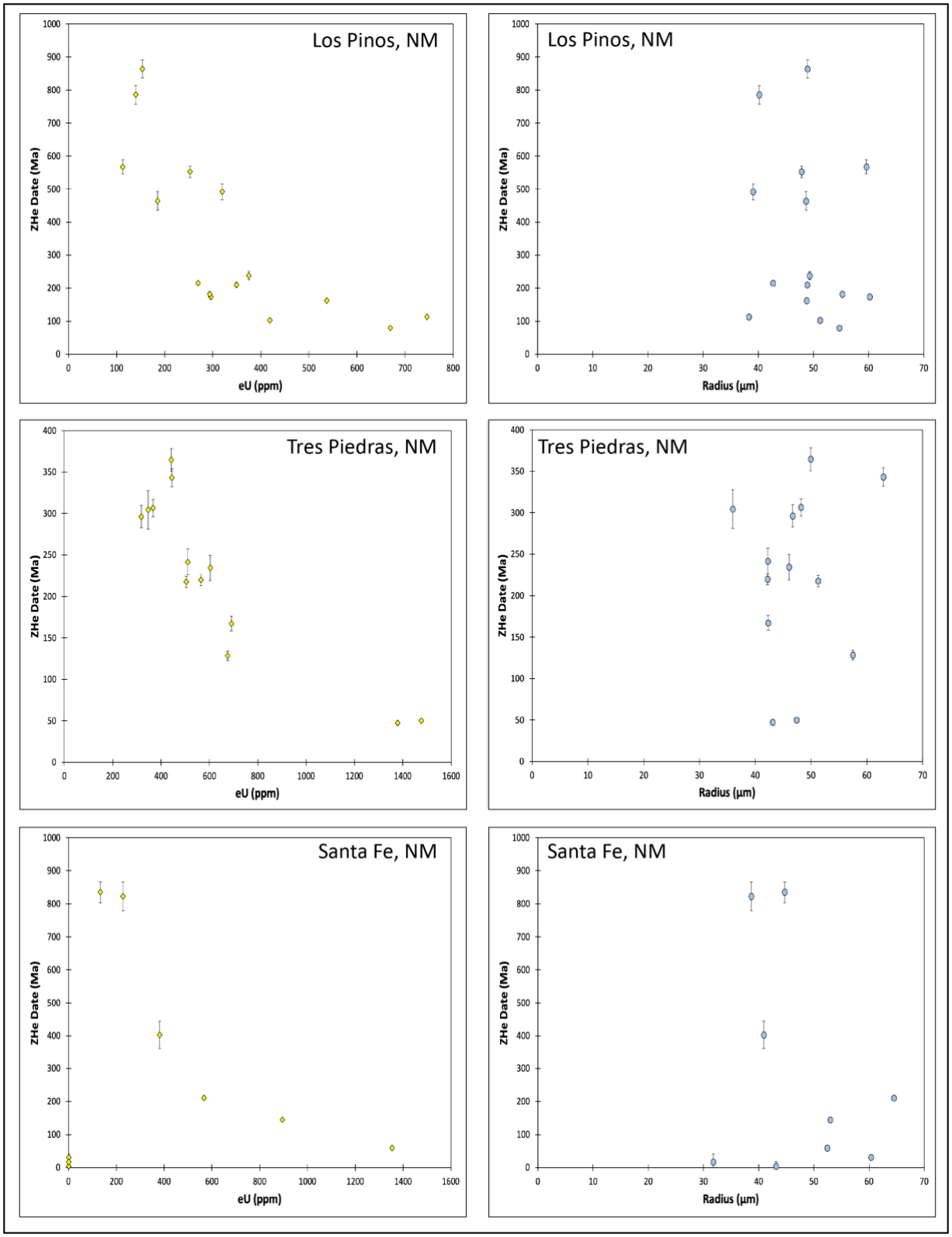

Figure 8: eU vs. zircon (U-Th)/He date and radius vs. zircon (U-Th)/He date plots for Los Pinos, Tres Piedras, and Santa Fe. Date uncertainties are 2σ.

from 0.7 – 1353.2 ppm (Fig. 6). A clear negative correlation between ZHe date and eU can be made, but no trend is observed between the ZHe date and radius (Fig. 8).

Sandia Mountains, New Mexico

Six ZHe dates from one Precambrian granite sample from the Sandia Mountains were presented by *Ault et al*. (2018). The ZHe dates obtained from these six grains showed a wide spread in ZHe date with values ranging from a 67-555 Ma. The eU content of these grains resulted in a large spread as well with the concentration ranging from 100-1175 ppm (Fig. 9). Overall, ZHe dates from this sample show a well-defined negative trend with eU. Additionally, no correlation is observed between the date and recorded radius of the grains (Fig. 9).

Front Range, Colorado

Eight ZHe dates obtained from the Precambrian granodiorite below the GU in the Front Range, CO were presented by *Ault et al*. (2018). The ZHe dates from this sample resulted in relatively young dates and fell within a narrow range with values spanning 55.2-122 Ma. The eU concentration of these grains displayed a larger range with values from 342-878 ppm (Fig. 9). A clear negative correlation between ZHe date and eU can be made, but no trend is observed between the ZHe date and radius (Fig. 9).

4.3 Forward Models

Forward models constructed for the three newly collected samples were used to test the two different cooling scenarios displayed in Figure 1. For each scenario twelve individual time-temperature paths were examined resulting in a total of 24 t-T paths modeled for Los Pinos, Tres

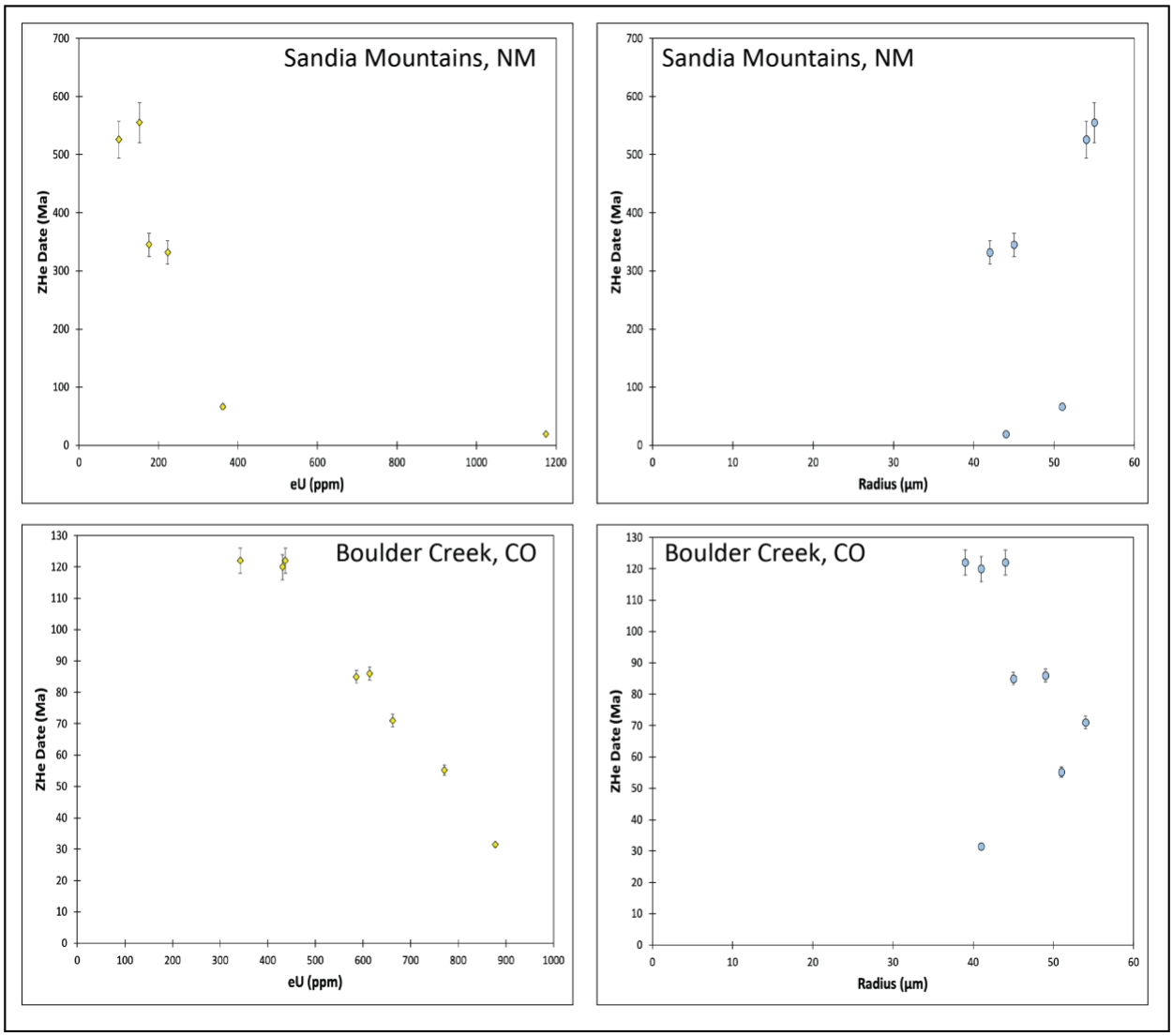

Figure 9: eU vs. zircon (U-Th)/He date and radius vs. zircon (U-Th)/He date plots for Sandia Mountains and Boulder Creek, CO. Date uncertainties are 2σ. Data are compiled from *Ault et al.* (2018).

Piedras, and Santa Fe samples. Scenario 1 tests the simple unconformity hypothesis, and includes three separate Precambrian cooling paths. In the first path (green in Fig. 10) the sample remains buried after crystallization and is rapidly cooled to the surface immediately prior to formation of the GU. The second path (blue path in Fig. 10) represents gradual cooling throughout the Precambrian until it reached surface temperatures. Finally, the third path (red path in Fig. 10) involves rapid exhumation after crystallization and then prolonged residence at surface temperatures until the formation of the GU. For all three paths in scenario 1 four different paths were tested that varied the depth of burial after the GU in intervals of 20 °C.

Additional forward model paths were constructed to test scenario 2, where the GU is a compound unconformity. For these paths the sample is cooled to surface temperatures at 1400 Ma, and is then reheated to varying temperatures. Once again three distinct scenarios were tested with each varying the duration of burial and timing of exhumation prior to the formation of the GU. Within the three scenarios four paths were tested that varied the depth of burial in intervals of 10 °C.

These rough forward models can then be used to test viable thermal histories by comparing the calculated ZHe date-eU curve to the ZHe date results for each sample (Table 2). Below are the results of the forward models for Los Pinos, Tres Piedras, and Santa Fe.

Los Pinos Mountains, New Mexico

For the first set of 12 paths three scenarios were examined for the Los Pinos Mountains. The first four paths tested whether the sample remained buried throughout the Precambrian and was rapidly exhumed right before the formation of the GU. For these four paths the crystallization age was set at 1660 Ma and was then held at 700 °C until 330 Ma at which point it

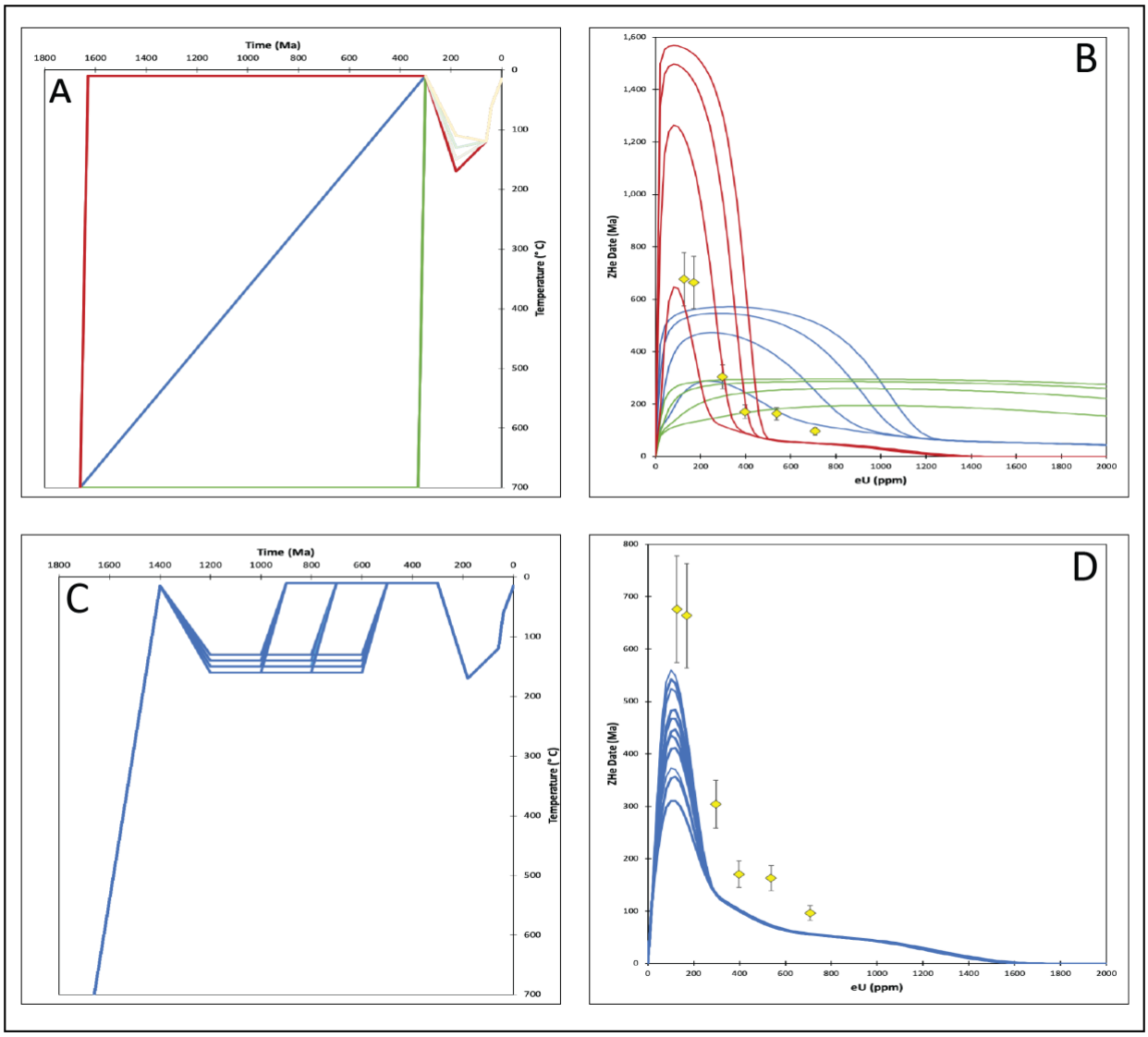

Figure 10: Hypothetical time-temperature paths and corresponding eU vs. ZHe data plots for Los Pinos Mountains, NM. A and B test whether the sample could have remained buried until the formation of the GU, a gradual uplift scenario, or whether the sample was rapidly exhumed to the surface and sat undisturbed. C and D test for possible reburial during the Precambrian and vary the timing of exhumation and depth of reburial. Yellow diamonds are the ZHe data points for the sample. Note that none of the paths tested yield ZHe date vs. eU curves that match the data.

was rapidly exhumed to the surface (Fig. 10) (*Shastri & Bowring* 1992). This was followed by a period of reburial at 180 to temperatures ranging between 170-110 °C and then exhumed to 120 °C by 60 Ma, 60 °C by 40 Ma, and finally 15 °C at present day consistent with apatite fission track ages and thermal history modeling from that location (*Kelley et al.* 1992). The corresponding age-eU curves were very similar to one another, and the oldest predicted ZHe dates are no higher than 300 Ma (Fig. 10B). Additionally, all four curves remained consistent in ages across eU content resulting in very broad curves.

The next four paths were designed to test whether the sample experienced a gradual cooling period from time of crystallization to the formation of the GU. Once again, the age of crystallization was set at 1660 Ma at 700 °C, but the sample was allowed to gradually cool to surface temperatures until 300 Ma (Fig. 10). The four paths in this scenario produced ZHe date-eU curves that predict maximum ZHe dates that vary from ~300—600 Ma. All four curves include broad peaks until eU values of 600 ppm, at which point the ZHe dates drastically fell until all four became synchronous at eU values of 1200 ppm (Fig. 10).

The final four paths in set one of the forward models for Los Pinos examined whether the sample could have resided at the surface for a prolonged period of time undisturbed. For this set of paths, the crystallization age was set at 1660 Ma at 700 °C. The sample was then exhumed to surface temperatures of 10 °C by 1630 Ma and then remained at this temperature until 300 Ma when it was reburied as in the previous two sets. The resulting ZHe date-eU curves predicted the oldest ZHe dates, ranging from ~650—1550 Ma (Fig. 10B). All four curves show a rapid drop in ZHe dates after they peak until they all reach the same ZHe ages at eU values of 500 ppm (Fig. 10B).

For the second set of forward models an additional 12 t-T paths were constructed to explore the possibility of a compound unconformity, including multiple periods of burial and exhumation prior to the formation of the GU. For all 12 paths the crystallization age was set to 1660 Ma at 700 °C and was then rapidly exhumed to surface temperatures by 1400 Ma (Fig. 10A). The sample is then immediately reburied to various temperatures. Three scenarios were then tested that varied the timing of exhumation by intervals of 200 Ma. The first set of paths was exhumed from 1000—900 Ma, the second set was exhumed from 800—700 Ma, and the third set was exhumed from 600—500 Ma (Fig. 10C). Additionally, for each set the depth of burial was varied and ranged from 130-160 °C. The age-eU curves produced by these t-T paths resulted in a maximum ZHe date of 550 Ma and a low of 300 Ma (Fig. 10D). All the curves show a steep drop in ZHe date after reaching their maximum until they all became synchronous at eU values of 300 ppm. None of the ZHe date-eU curves produced yield a good correlation with the observed ZHe data points for this sample (Fig. 10).

Tres Piedras, New Mexico

For the first set of 12 paths tested for Tres Piedras three scenarios were examined. The first four paths examined whether the sample may have been buried for a prolonged period of time prior to formation of the GU. The crystallization age was set to 1650 Ma at 700 °C and the sample remained at high temperatures until 535 Ma at which point it was rapidly exhumed to surface temperatures of 15 °C by 515 Ma (Fig. 11). The sample was then reburied to temperatures ranging from 170-110 °C at 180 Ma and then exhumed to surface temperatures at present day. The ZHe date-eU curves produced from these four paths show a maximum ZHe date of 500 Ma and a low of 250 Ma. Additionally, all four paths remained relatively consistent in ZHe date across eU values producing very broad curves (Fig. 11). When compared to the

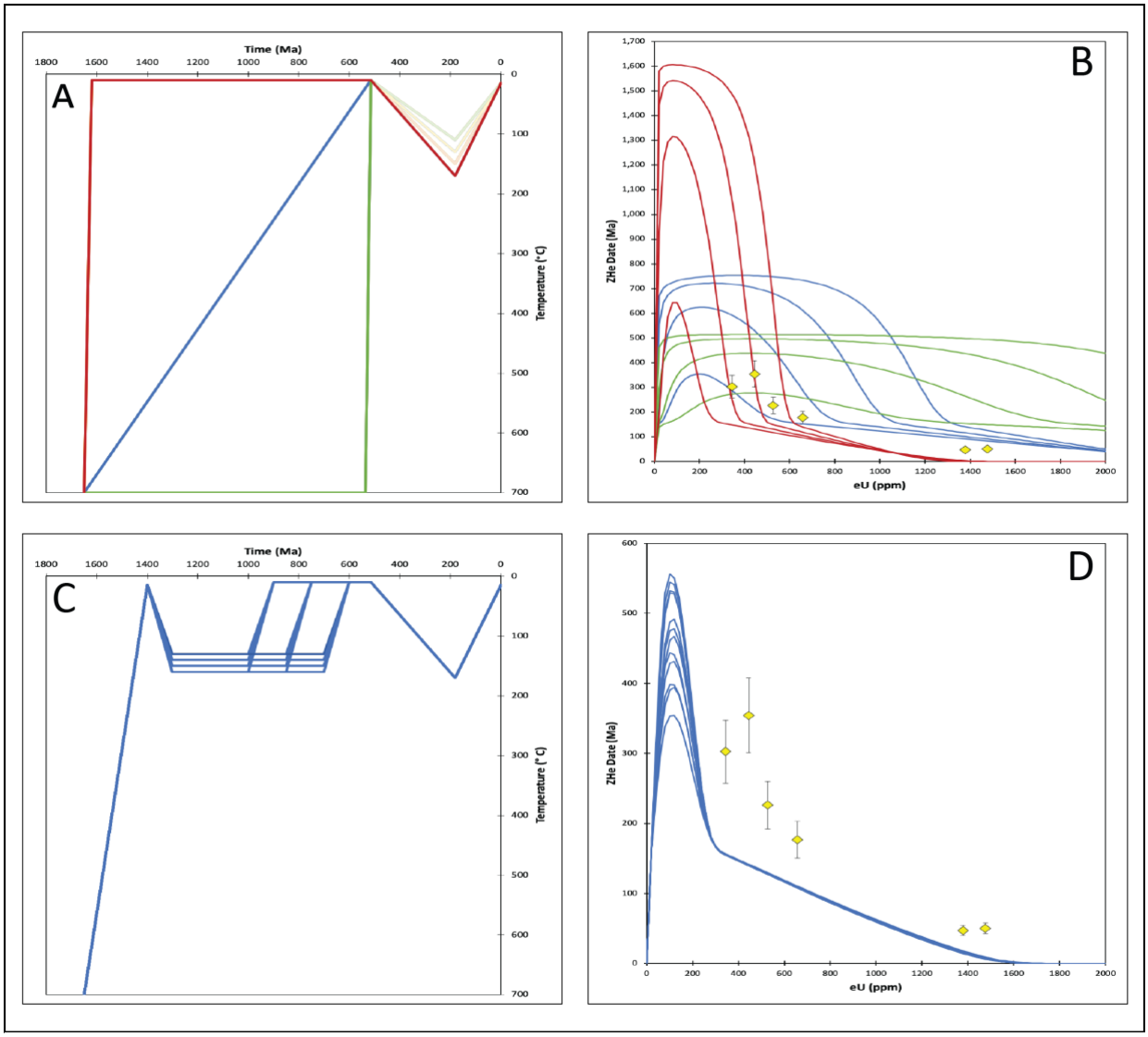

Figure 11: Hypothetical time-temperature paths and corresponding eU vs. ZHe data plots for Tres Piedras, NM. A and B test whether the sample could have remained buried until the formation of the GU, a gradual uplift scenario, or whether the sample was rapidly exhumed to the surface and sat undisturbed. C and D test for possible reburial during the Precambrian and vary the timing of exhumation and depth of reburial. Yellow diamonds are the ZHe data points for the sample. Note that none of the paths tested yield ZHe date vs. eU curves that match the data.

ZHe data obtained for this sample none of these eU curves could be correlated with the data (Fig. 11).

The second four paths allowed for the sample to cool gradually through time until it reached surface temperatures of 15 °C at 515 Ma, consistent with the observed unconformity of the Cambrian Bliss Formation overlying the Precambrian Granite (Fig. 11) (*Amato & Mack,* 2012). From this point the sample was then reburied to temperatures ranging from 170-110 °C at 180 Ma and then exhumed to surface temperatures at present day. The corresponding ZHe date-eU curves for these four paths reached a maximum ZHe date of 750 Ma and a low of 350 Ma (Fig. 11B). All four curves have broad peaks until they start to gradually decline in ZHe date up to eU values of 1400 ppm. From this point all four curves become relatively consistent with one another. When comparing the age-eU curves to the recorded ZHe data points for the sample none of the paths can be correlated with the data (Fig. 11B).

The final four paths in this set of forward models are rapidly exhumed to surface temperatures of 10 °C by 1620 Ma in order to test whether this sample was exhumed and then resided at surface temperatures for a prolonged period of time. All four paths remain at surface temperatures until 515 Ma. The resulting ZHe date-eU curves produced by these four paths yield maximum ZHe dates that range from 650—1600 Ma. All four paths show a steep negative slope as ZHe dates drastically fall until they all became synchronous at eU values of 900 ppm (Fig. 11B).

The second set of 12 paths were constructed to test scenario 2, a compound unconformity. For all 12 paths the age of crystallization was set to 1650 Ma at 700 °C, and the paths are then forced to surface temperatures by 1400 Ma and then buried. Three scenarios were then tested that varied the timing of exhumation by intervals of 200 Ma. The first set of paths

was exhumed from 1000—900 Ma, the second set was exhumed from 800—700 Ma, and the third set was exhumed from 600—500 Ma (Fig. 11C). Additionally, for each scenario the depth of burial was varied from 130-160 °C in intervals of 10 °C. The age-eU curves produced by these 12 t-T paths were similar to one another and reached a maximum ZHe date of 550 Ma and a low of 350 Ma (Fig. 11D). After reaching maximum ZHe dates the curves rapidly drop, forming a narrow peak until all paths became synchronous at eU values of 300 ppm. When compared to the ZHe data obtained for this sample none of the age-eU curves produced can be correlated to the data (Fig. 11).

Santa Fe, New Mexico

The first set of 12 paths constructed for the Santa Fe sample test variations of scenario 1, the simple unconformity model. The first set examines whether a prolonged period of burial was likely throughout the Precambrian. In this set the crystallization age was set to 1680 Ma at a temperature of 700 °C and then held at this temperature until 360 Ma where it was rapidly exhumed to 15 °C by 340 Ma (Fig. 12A). After this the sample was then reburied to temperatures ranging between 120-180 °C at 50 Ma, followed by cooling to 90 °C at 40 Ma, 30 °C by 10 Ma, and finally surface temperatures at present day. The 50-0 Ma thermal history constraints for this sample come from published apatite fission-track ages and thermal history modeling (*Kelley et al*. 1992). The ZHe date-eU curves produced by these four paths indicate maximum ZHe dates that range from 100—300 Ma (Fig. 12B). Additionally, all four curves remained consistent across all values of eU with respect to ZHe date, resulting in broad curves.

The second four paths tested gradual cooling throughout the Precambrian. For these paths the crystallization age was set to 1680 Ma at a temperature of 700 °C and then allowed to

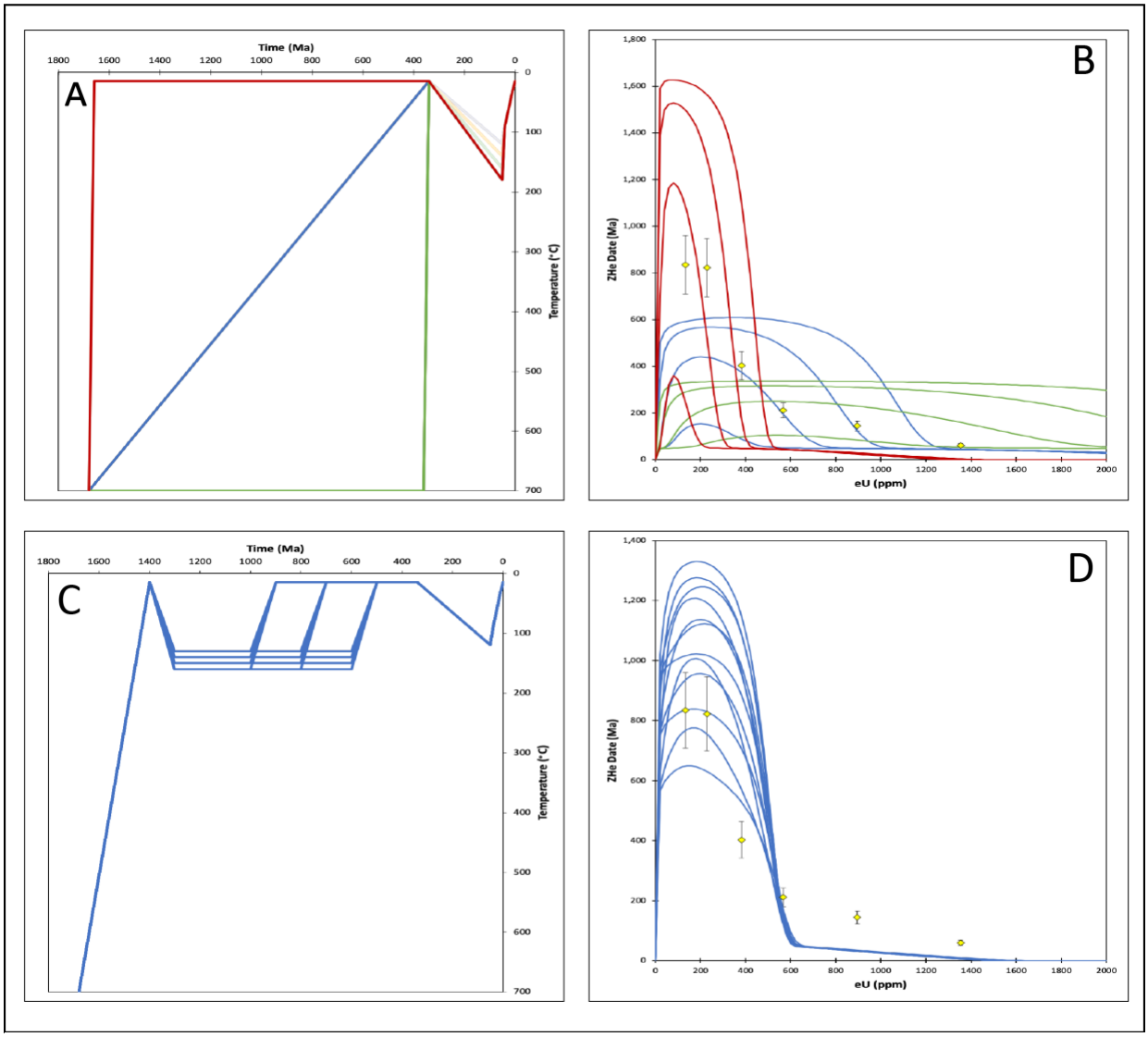

Figure 12: Hypothetical time-temperature paths and corresponding eU vs. ZHe data plots for Santa Fe, NM. A and B test whether the sample could have remained buried until the formation of the GU, a gradual uplift scenario, or whether the sample was rapidly exhumed to the surface and sat undisturbed. C and D test for possible reburial during the Precambrian and vary the timing of exhumation and depth of reburial. Yellow diamonds are the ZHe data points for the sample. Note that none of the paths tested yield ZHe date vs. eU curves that match the data.

gradually cool to surface temperatures of 15 °C until 340 Ma. The ZHe date-eU curves produced by these four paths yield maximum ZHe dates that range from 100—600 Ma (Fig. 12B). All four curves gradually dropped in ZHe dates until they coincide with one another at eU values of 1300 ppm (Fig. 12B).

The third set of paths in scenario 1 was created to examine whether the sample could have experience early cooling, followed by prolonged residence at the surface until the formation of the GU. For these four paths the crystallization age was set at 1680 Ma at a temperature of 700 °C. The sample was then forced to rapidly exhume to the surface by 1660 Ma at surface temperatures of 15 °C and was allowed to reside at the surface until 340 Ma when it began to be reburied (Fig. 12A). As in the previous sets of paths after 340 Ma then same constraints were applied to the sample. The ZHe date-eU curves that correspond to these paths reach a maximum ZHe date of about 1600 Ma with a minimum value of 350 Ma (Fig. 12B). All four curves dropped in ZHe values immediately after reaching their peak until they became synchronous at eU values of 500 ppm.

The second set of 12 paths tested for the possibility of burial and exhumation prior to the formation of the GU. Three different scenarios were examined that varied the timing of exhumation after burial. For all 12 paths the timing of crystallization was at 1680 Ma at 700 °C followed by being rapidly exhumed to surface temperatures by 1400 Ma (Fig. 12). Three scenarios were then tested that varied the timing of exhumation by intervals of 200 Ma. The first set of paths was exhumed from 1000—900 Ma, the second set was exhumed from 800—700 Ma, and the third set was exhumed from 600—500 Ma (Fig. 12) Additionally, for each scenario the depth of burial was varied from 130-160 °C in intervals of 10 °C. The age-eU curves produced by these paths reached a maximum ZHe date of 1300 Ma with a low of about 600 Ma (Fig. 12).

Immediately after reaching their peak all eU curves dropped in ZHe date values, and all 12 curves became synchronous at eU values of 600 ppm. When compared to the recorded ZHe data points for this sample none of the eU curves can be correlated to all of the data points (Fig. 12).

4.4 Inverse Models

Inverse modeling was utilized in this study due to its ability to easily test thousands of possible t-T paths compared to the tens of possible paths analyzed in the forward modeling. Additionally, inverse modeling can examine any possible t-T path that matches measured thermochronometric ages within a specific error compared to the overly simplistic t-T paths examined in the forward models. Overall the inverse models created are used to further refine the possible thermal histories of the samples.

Inverse models are presented for Los Pinos Mountains, NM, Tres Piedras, NM, Santa Fe, NM, Sandia Mountains, NM, and Front Range, CO. For all five samples, inverse models were produced to test between the two main scenarios. The first inverse model was constructed to test scenario 1, where the sample cools after crystallization until formation of the GU. The second inverse model was constructed to test scenario 2, which includes a period of Precambrian reburial and exhumation prior to formation of the GU. Presented below are the inverse model results for each of the five locations.

Los Pinos Mountains, New Mexico

Six synthetic grains from the Los Pinos Mountains sample 89LP08 were ran in HeFTy with a 15% age uncertainty (see table 1 for complete modeling assumptions and input data). The six synthetic grains were created by binning the ZHe data from the sample according to observed clusters of ZHe grains that plot in similar locations (Fig. 13). Along with the synthetic grain

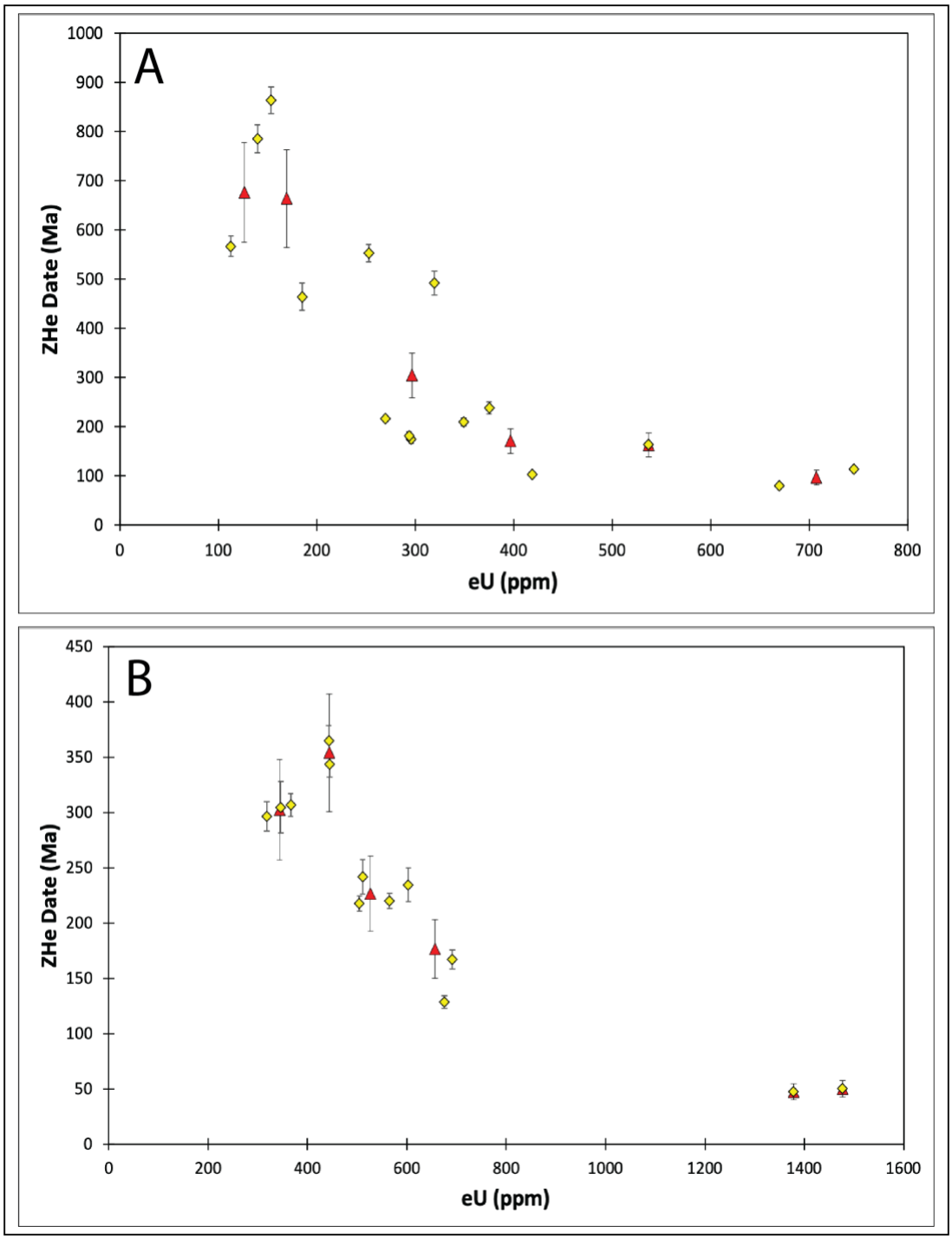

Figure 13: **A.** Comparison between the synthetic vs. original ZHe data points for Los Pinos Mountains, NM. **B.** Comparison between the synthetic vs. original ZHe data points for Tres Piedras, NM. Yellow diamonds are the original ZHe data points and red triangles are the synthetic grains created for thermal modeling analysis. Date uncertainties for yellow ZHe dates are 2σ. Date uncertainties for red ZHe dates are 15% error margin.

information the same geologic constraints utilized in the forward modeling were input into HeFTy to create the inverse models. Additional constraint boxes were applied in the reburial scenario in order to test for reburial during the Precambrian. This included a constraint box that allowed for rapid exhumation by 1600-1500 Ma between temperatures of 45-10 °C after crystallization (Fig. 14). This is followed by a large constraint box between 1500-320 Ma with temperatures ranging from 300-35 °C in order to allow for burial prior to the formation of the GU (Fig. 14).

For the gradual scenario the model resulted in 61 acceptable paths and 12 good paths. Four of the paths suggest that after crystallization the sample is rapidly exhumed to near-surface temperatures between 1400-1200 Ma, and then resides at low temperatures until the formation of the GU (Fig. 14). However, the remaining eight paths suggest that the sample reached temperatures of about 180 °C by 1200 Ma, and from this point gradually cooled until they reach surface temperatures between 600-400 Ma (Fig. 14).

Thermal modeling results for the Los Pinos Mountains reburial scenario produced 147 acceptable paths and 10 good paths (Fig. 14). The model suggests that after rapid exhumation the sample begins to be buried starting at 1400 Ma and reaches a maximum reburial temperature of 250 °C between 1000-900 Ma (Fig. 14). The model then suggests that most paths start to be exhumed by 800 Ma and reach surface temperatures between 600-400 Ma. Only one path reaches surface temperatures any earlier by 900 Ma (Fig. 14).

Tres Piedras, New Mexico

Six synthetic grains from the Tres Piedras sample 18TUS03 were ran in HeFTy with a 15% uncertainty. The six grains were created by binning the ZHe data from the sample according to observed clusters of ZHe grains that plotted in similar locations (Fig. 15). Once the synthetic

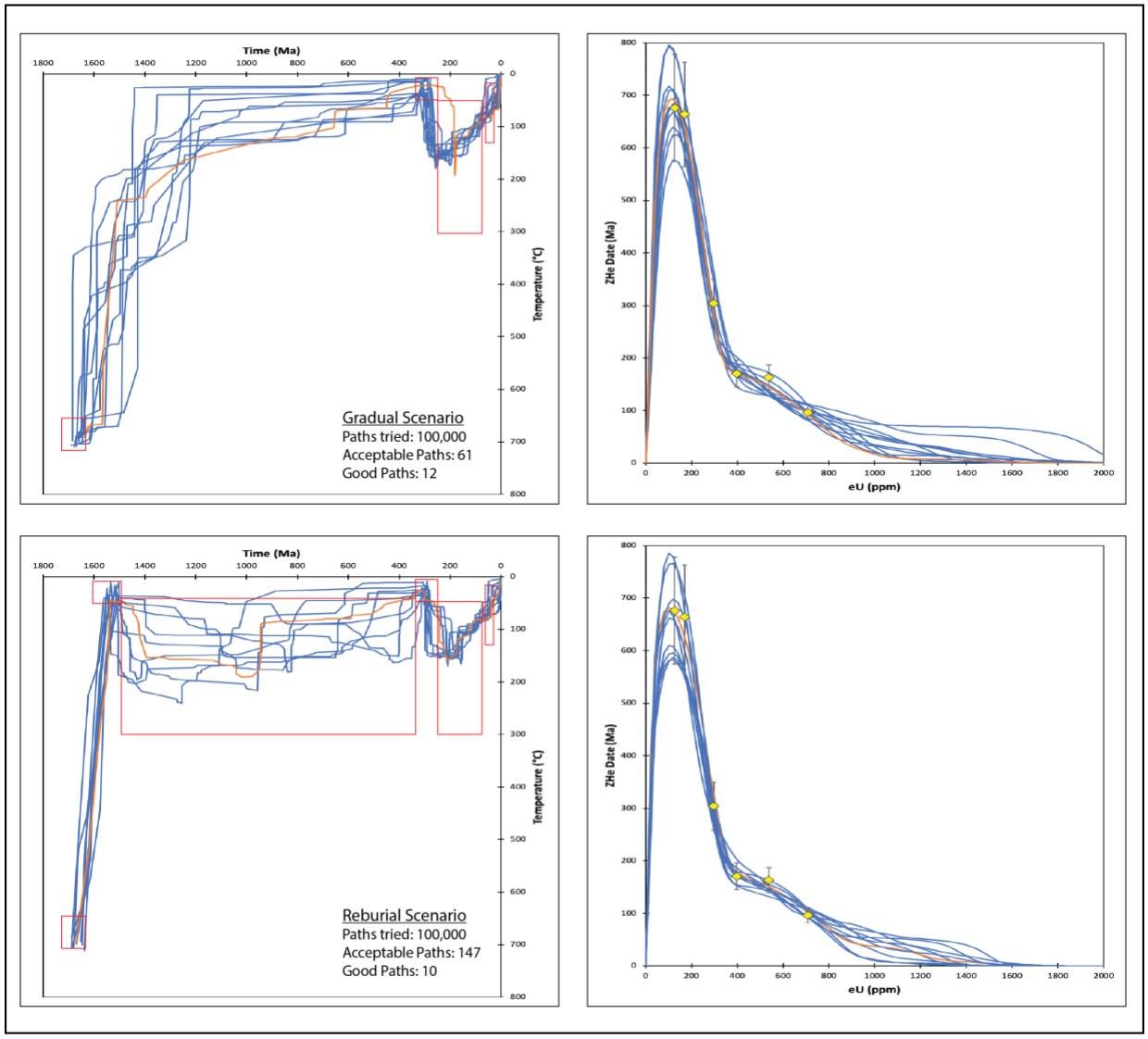

Figure 14: Inverse model results for Los Pinos Mountains, NM. Time-temperature windows in the left column show good time-temperature paths in blue with the best fit path highlighted in orange. eU vs. ZHe data plots on the right show data used in the thermal history modeling in yellow. Each blue curve represents the predicted eU-date correlation that corresponds to one of the good paths that resulted from the inverse model, where the orange curve highlights the best fit curve to the data. Red outlined boxes in the time-temperature windows represent the constraints that were applied to each scenario.

grain information was inputted into HeFTy the same geologic constraints used in the forward modeling were applied as well for both scenarios. Additional constraints were applied to the reburial scenario model in order to test for the possibility of burial and exhumation occurring prior to the formation of the GU. The first supplementary constraint was set from 1590-560 Ma between temperatures of 25-5 °C to bring the sample to surface temperatures after crystallization. This was followed by another constraint box from 1530-560 Ma between temperatures of 300-10 °C in order to allow for the possibility of burial prior to the formation of the GU (Fig. 15).

The results for the gradual scenario resulted in 122 good paths and 39 good paths. The model suggests that after crystallization the sample gradually cools through a wide range of temperatures over time (Fig. 15). The earliest any paths reach surface temperatures begins at 800 Ma. While the majority of the 39 paths reach surface temperatures between 600-500 Ma (Fig. 15).

Thermal modeling results for the reburial scenario produced 31 acceptable paths and 3 good paths. The model suggests that after being rapidly exhumed to the surface the sample begins to be buried by 1400 Ma and reaches a maximum burial temperature of about 300 °C by 1300 Ma (Fig. 15). All paths then suggest that starting at 700 Ma the sample begins to be exhumed to the surface and reaches surface temperatures by 550 Ma (Fig. 15).

Santa Fe, New Mexico

Six grains were utilized from sample 18NC01 for the Santa Fe, NM sample. All grain information was inputted into HeFTy with a 15% age uncertainty along with the previously utilized geologic constraints for the sample. Additional constraints were applied to the reburial scenario in order to allow for the possibility of burial during the Precambrian. First, an additional constraint box was applied after crystallization between 1600-1500 Ma with temperatures

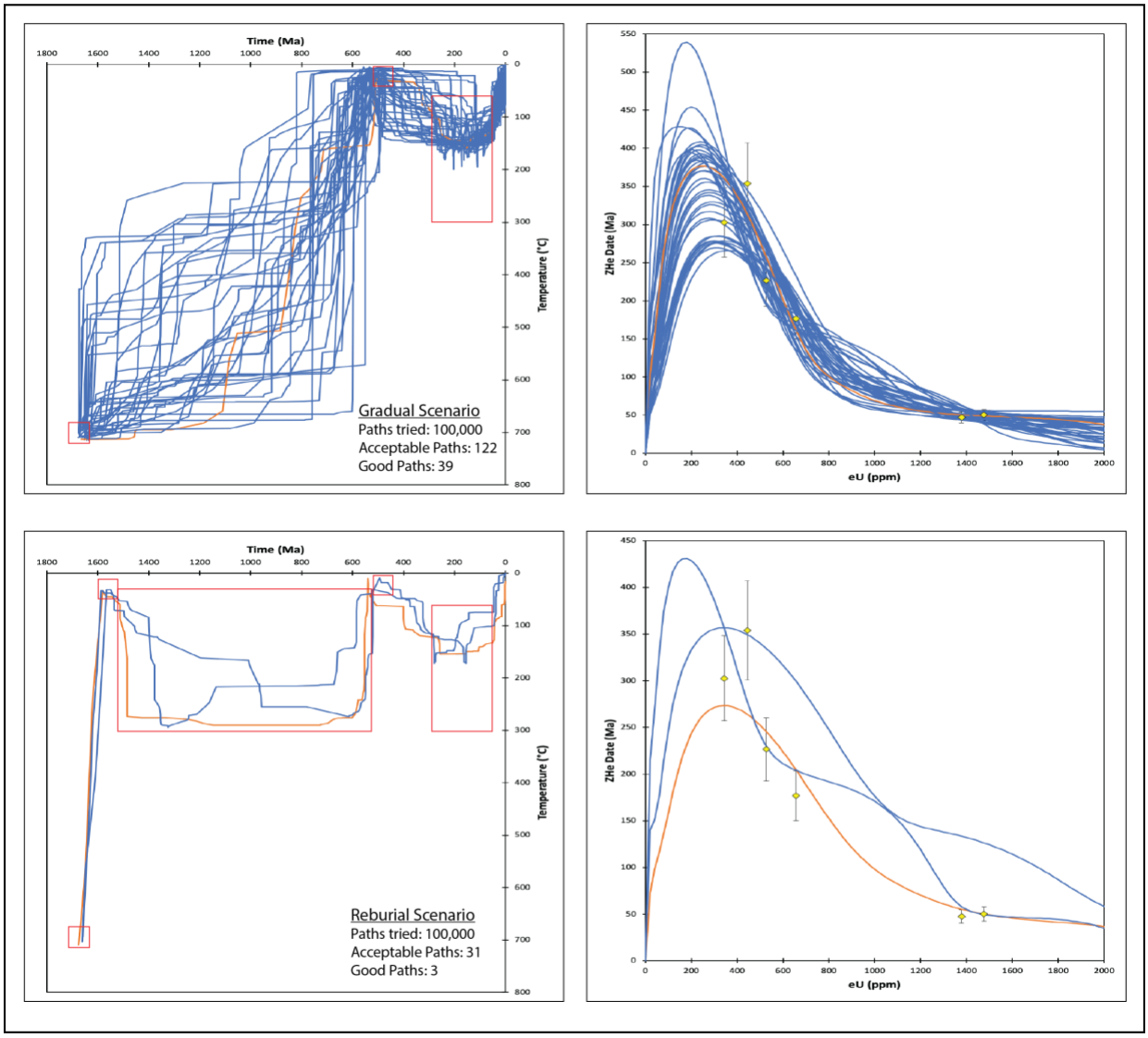

Figure 15: Inverse model results for Tres Piedras, NM. Time-temperature windows in the left column show good time-temperature paths in blue with the best fit path highlighted in orange. eU vs. ZHe data plots on the right show data used in the thermal history modeling in yellow. Each blue curve represents the predicted eU-date correlation that corresponds to one of the good paths that resulted from the inverse model, where the orange curve highlights the best fit curve to the data. Red outlined boxes in the time-temperature windows represent the constraints that were applied to each scenario.

ranging from 25-5 °C in order to exhume the sample to the surface (Fig. 16). Another constraint was then set between 1500-360 Ma between 300-50 °C in order to allow for burial prior to the formation of the Great Unconformity (Fig. 16).

Results for the gradual scenario produced 30 acceptable paths and 7 good paths. Two of the paths gradually cool and reach surface temperatures at 950 Ma. While the remaining five good paths suggest that the sample does not reach surface temperatures until 600-500 Ma (Fig. 16).

The results for the reburial scenario thermal model produced 2 acceptable paths and 1 good path. The sole good path suggests that after rapid exhumation to the surface the sample begins reburial at 1500 Ma and reaches a maximum reburial temperature of 250 °C at 1100 Ma (Fig. 16). After this the model suggests that begins to be exhumed at 950 Ma and reaches surface temperatures at 800 Ma (Fig. 16).

Sandia Mountains, New Mexico

The Sandia Mountains inverse models utilized data originally collected by *Ault et al.* (2018) from sample MC14-s6. A total of six grains were ran in HeFTy with a 15% age uncertainty. In addition to the grain information that was collected additional parameters were applied to the model according to known geologic constraints. The crystallization age for the sample was set at >600 °C at 1400 Ma and then rapidly cooled to 10 °C by 1300 Ma to account for the unroofing event related to the Grenville orogeny (*Ault et al.* 2018). The next known constraint was at 550 Ma where it was known to be at surface temperatures of 10 °C due to Precambrian-Mississippian regional unconformity and then reburied at 400 Ma to 100 °C (Fig. 17). The sample was then exhumed to the surface by 300 Ma in accordance with the observed Pennsylvanian San Andreas and Madera Formations unconformably overlying the Sandia

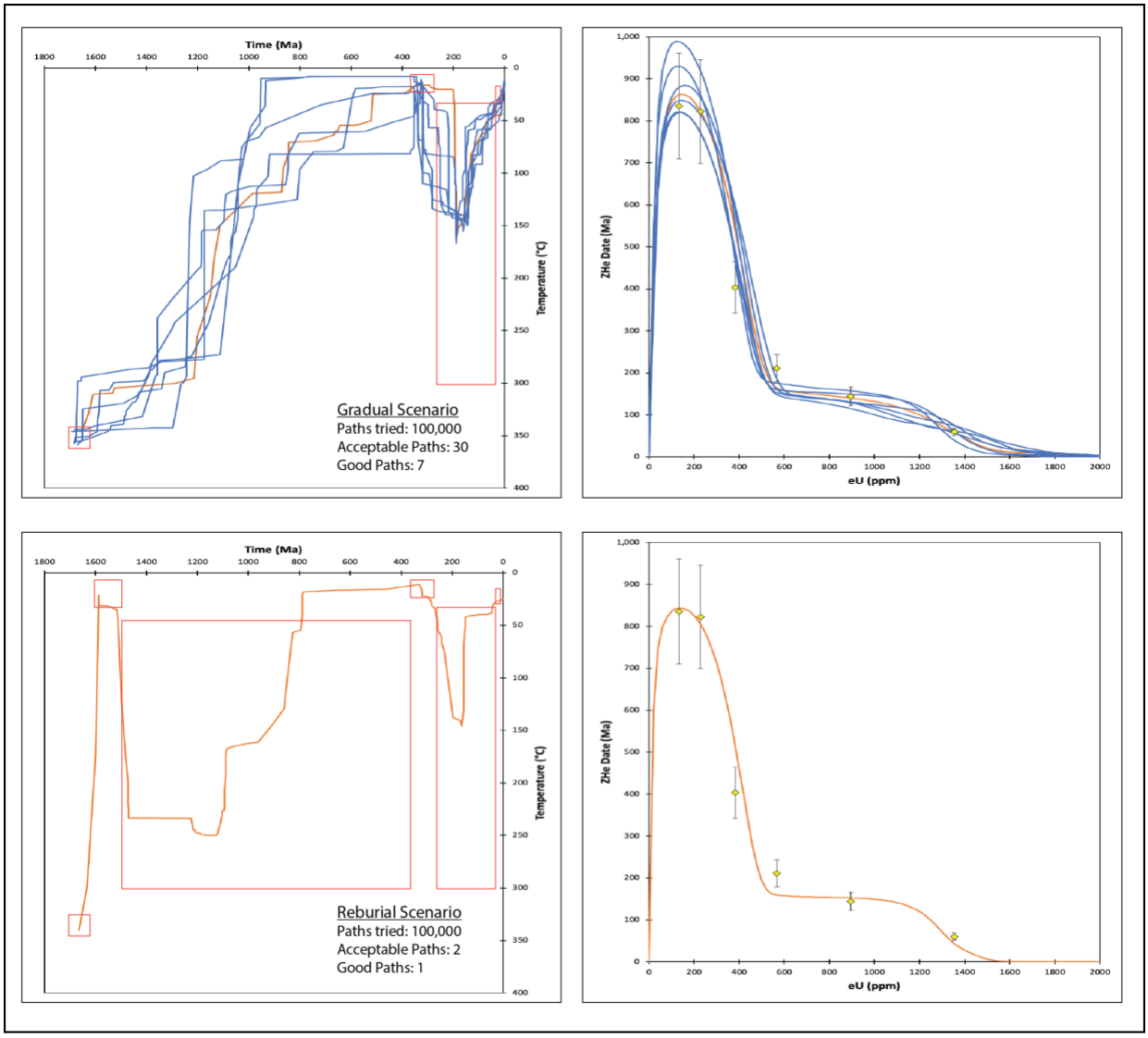

Figure 16: Inverse model results for Santa Fe, NM. Time-temperature windows in the left column show good time-temperature paths in blue with the best fit path highlighted in orange. eU vs. ZHe data plots on the right show data used in the thermal history modeling in yellow. Each blue curve represents the predicted eU-date correlation that corresponds to one of the good paths that resulted from the inverse model, where the orange curve highlights the best fit curve to the data. Red outlined boxes in the time-temperature windows represent the constraints that were applied to each scenario.

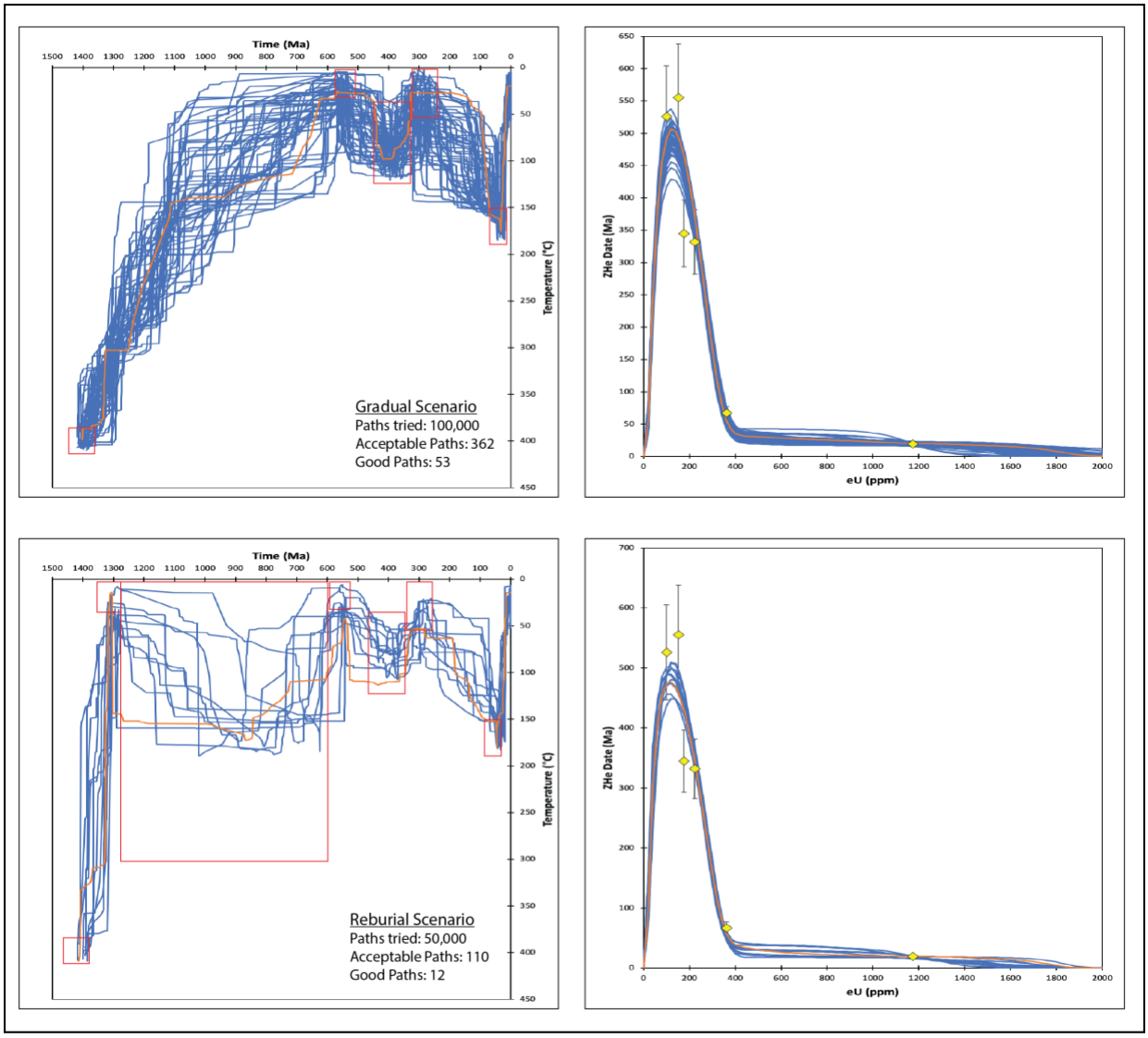

Figure 17: Inverse model results for Sandia Mountains, NM. Time-temperature windows in the left column show good time-temperature paths in blue with the best fit path highlighted in orange. eU vs. ZHe data plots on the right show data used in the thermal history modeling in yellow. Each blue curve represents the predicted eU-date correlation that corresponds to one of the good paths that resulted from the inverse model, where the orange curve highlights the best fit curve to the data. Red outlined boxes in the time-temperature windows represent the constraints that were applied to each scenario.

granite. Then reheated to 170 °C by 20 Ma and rapidly cooled to 20 °C by 10 Ma consistent with apatite He date-eU patterns (*Ault et al.* 2018). Finally, in order to test whether the sample could have experienced a period of reburial prior to the GU a large constraint was placed from 1300-550 Ma between temperatures of 10-200 °C in the reburial scenario model (Fig. 17).

The thermal modeling for the gradual scenario resulted in 362 acceptable paths and 53 good paths. The model suggests that after crystallization the sample gradually cools to the surface and the earliest any paths reach surface temperatures occurring at 900 Ma (Fig. 17). Although the majority of paths in this model suggest that the sample does not reach surface temperatures until 700-550 Ma (Fig. 17).

The reburial scenario model resulted in 110 acceptable paths and 12 good paths. The model suggests that after crystallization and rapid exhumation to the surface the sample begins to be reburied at 1200 Ma (Fig. 17). The model then suggests that the sample is buried to a maximum temperature of 200 °C by 900 Ma. After this the sample begins to be exhumed to the surface and reaches surface temperatures between 650-550 Ma (Fig. 17).

Front Range, Colorado

The Front Range, CO inverse models utilized data originally collected by *Ault et al.* (2018) from sample A12-8. A total of seven grains were ran in HeFTy with a 15% age uncertainty. In addition to the grain information that was inputted additional parameters were applied to the model according to known geologic constraints. The crystallization age for the sample was set to >600 °C at 1700 Ma (Fig. 18). The following constraint forced the sample to cool to 300 °C by 1300 Ma in accordance with $^{40}Ar/^{39}Ar$ biotite thermochronology (*Ault et al.* 2018). The next two constraints were applied only to the reburial scenario in order to test for the

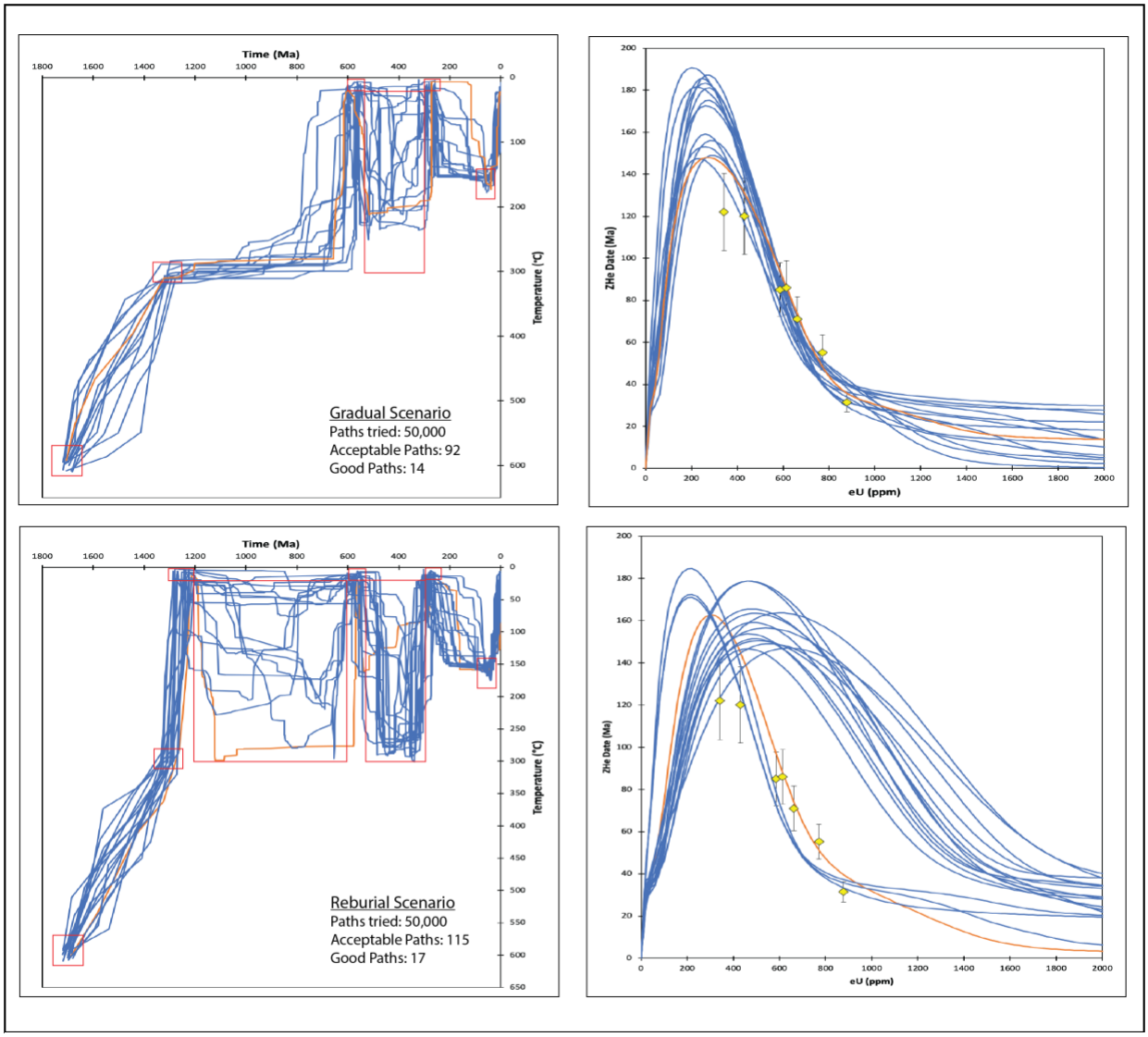

Figure 18: Inverse model results for Front Range, CO. Time-temperature windows in the left column show good time-temperature paths in blue with the best fit path highlighted in orange. eU vs. ZHe data plots on the right show data used in the thermal history modeling in yellow. Each blue curve represents the predicted eU-date correlation that corresponds to one of the good paths that resulted from the inverse model, where the orange curve highlights the best fit curve to the data. Red outlined boxes in the time-temperature windows represent the constraints that were applied to each scenario.

possibility of reburial prior to the formation of the GU. The first constraint forced the sample to surface temperatures between 1280-1200 Ma. Followed by a large constraint box from 1200-600 Ma from temperatures of 25-300 °C (Fig. 18). The constraints that follow are all known geologic constraints and were applied for both the gradual and reburial scenarios. These included cooling the sample to surface temperatures at ~550 Ma, and then reheating to 100 °C by ~400 Ma. The next constraint then cooled the sample to surface temperatures once again by ~300 Ma followed by reheating to temperatures of 150-175 °C at 60 Ma.

The gradual scenario model resulted in 92 acceptable paths and 14 good paths. The model suggests that after reaching a temperature of 300 °C at 1300 Ma the sample then remains at this temperature until ~800 Ma (Fig. 18). After this point the model suggests that the sample is rapidly exhumed and reaches surface temperatures by 650 Ma (Fig. 18).

The reburial scenario model resulted in 115 acceptable paths and 17 good paths. The model suggests that after reaching surface temperatures between 1280-1200 Ma the sample begins to be reburied and reaches a maximum reburial temperature of 300 °C (Fig. 18). The model then implies that the sample begins to be exhumed by ~800 Ma and reaches surface temperatures by 700 Ma (Fig. 18)

Chapter 5: Discussion

5.1 Gradual vs. Reburial Scenarios

The forward model results for all three new samples indicate that the Precambrian history is much more complex than the simplistic scenarios tested. This is apparent in the modeled date-eU curves produced from the t-T paths, where none of the curves yields a good match to the recorded ZHe dates from each sample (Fig. 10, 11, & 12). Due to these results, inverse modeling was then utilized in an attempt to further constrain the long-term thermal history of each sample.

Inverse modeling for all five samples resulted in good paths for both the reburial and gradual scenarios, indicating that either scenario is possible for each sample (Fig. 19). Although, the depth of burial observed in many of the reburial scenarios imply that the basins required to drive the samples to the maximum temperature recorded would have been of considerable thickness. The Los Pinos location gets reburied to a maximum temperature range of 100-250 °C, and the Front Range, CO sample is reburied to temperatures between 50-300 °C. All paths in the Tres Piedras, Santa Fe, and Sandia Mountains locations get reburied to the same temperature of 300 °C, 250 °C, and 200 °C respectively. When utilizing an assumed geothermal gradient of 25 °C/km this corresponds to a depth of 3.5-9.5 km for Los Pinos, 1.5-11 km for Front Range, 11 km for Tres Piedras, 9.5 km for Santa Fe, and 7.5 km for the Sandia Mountains (Fig. 19). These calculated burial depths can then be compared to the thickness of preserved Proterozoic deposits (Fig. 20). The Unkar and Chuar Groups within the Grand Canyon have a combined thickness of ~4 km (*Timmons et al.,* 2012). In Death Valley, the Pahrump Group is ~3 km thick (*Mahon et al*. 2014). The Apache Group in Arizona is ~0.5 km thick (*Shride,* 1967), and the Las Animas Formation in Colorado is ~1.3 km thick (*Tweto* 1983). None of these Proterozoic sedimentary

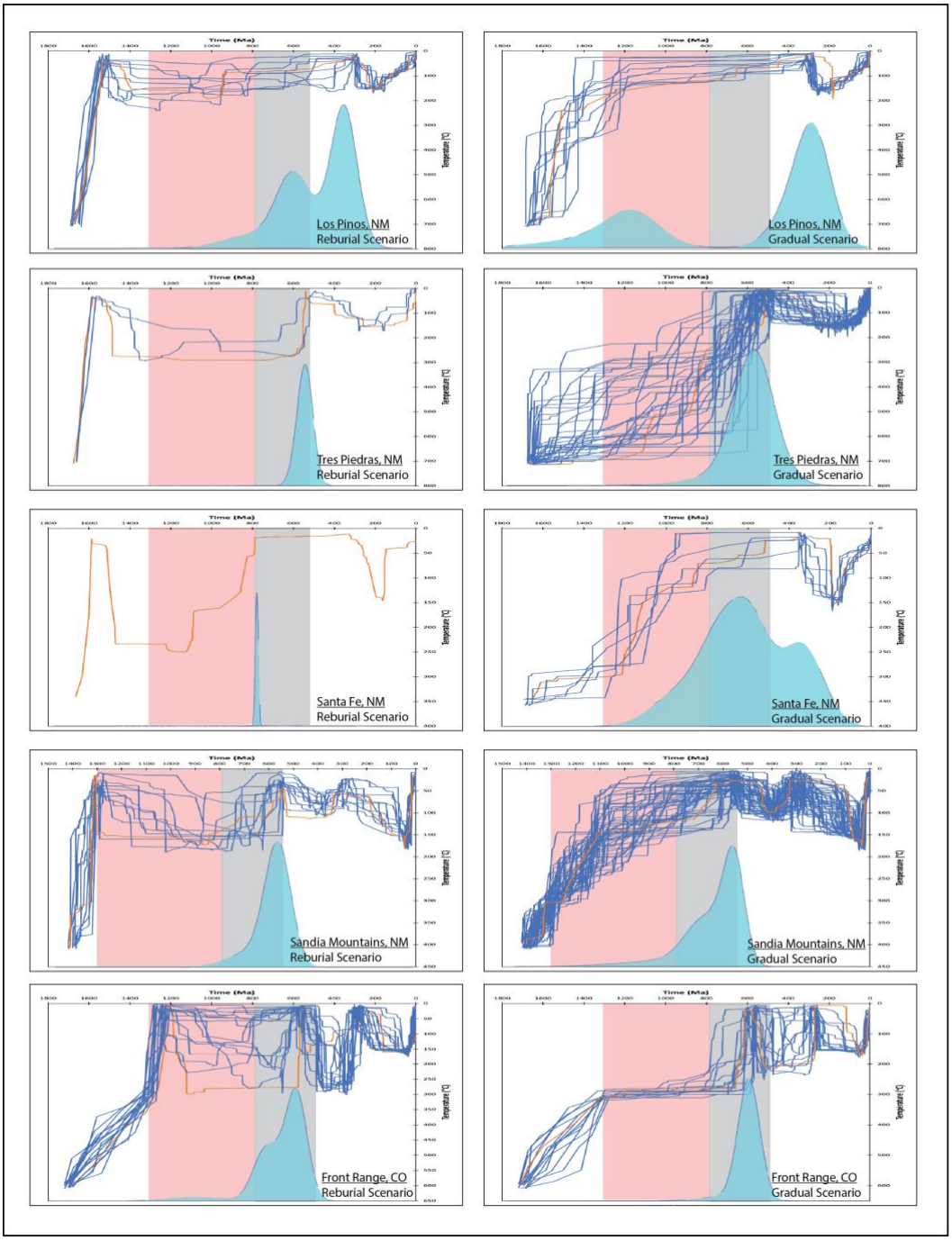

Figure 19: Comparison of the inverse model results for all samples. Left column showcases the results for the reburial scenario models and the right column showcases the results for the gradual scenario models. Highlighted in grey is the timing of the breakup of supercontinent Rodinia (ca. 0.78-0.55 Ga). Highlighted in red is the timing of assembly of Rodinia (ca. 1.3-0.78 Ga). The blue density plots show the number of t-T paths that cooled below 40 °C at a given time.

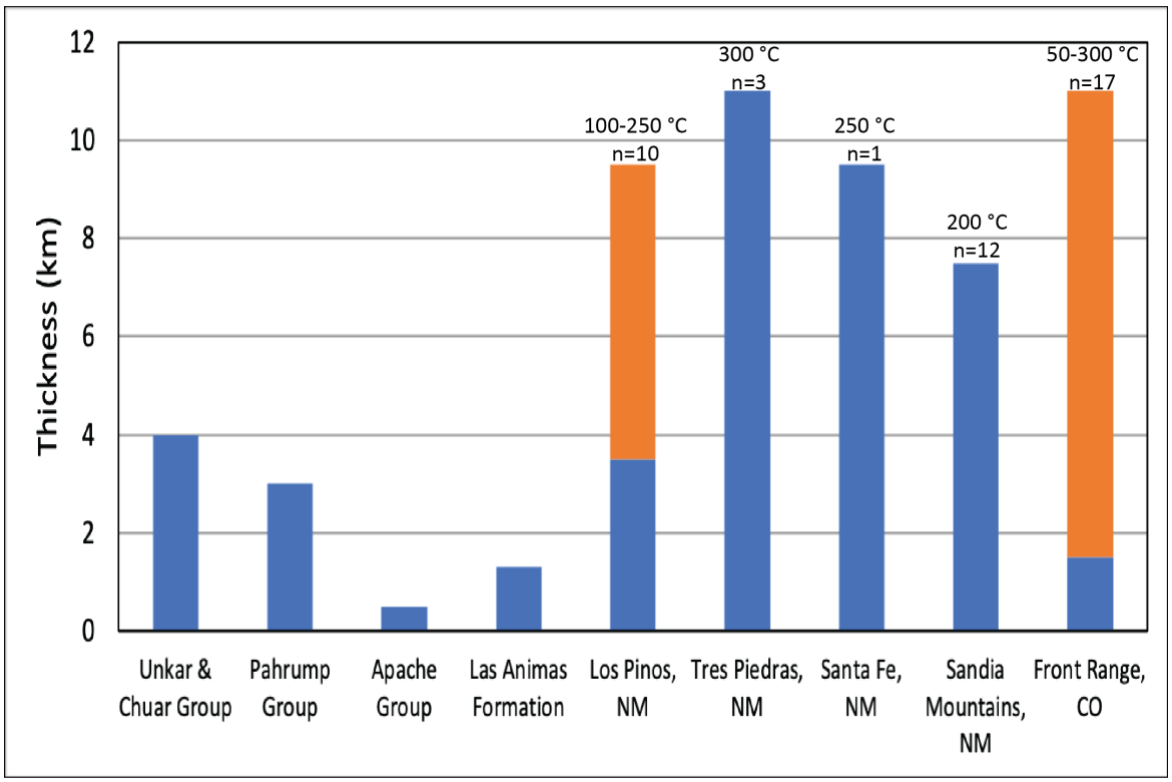

Figure 20: Existing Proterozoic sedimentary deposit thicknesses vs. hypothetical thickness of sedimentary basins needed to bury analyzed samples to depths recorded in reburial inverse models. For the Los Pinos Mountains and Front Range, CO locations the blue corresponds to the minimum thickness and the orange corresponds to the maximum thickness recorded in the reburial inverse models. The Tres Piedras, Santa Fe, and Sandia Mountains locations all get reburied to the same depth so the blue represents the thickness of the corresponding hypothetical basin. Above each plot of the samples analyzed in this study is the temperature range for reburial and the number of good t-T paths used in this analysis.

deposits exceed a thickness of four kilometers. Figure 20 compares the thicknesses of existing Proterozoic sedimentary deposits to the calculated thicknesses of a basin necessary to bury each sample to the depths recorded in the reburial inverse models. For the Tres Piedras, Santa Fe, and Sandia Mountains samples, all t-T paths get reheated to approximately the same temperature in the inverse models, corresponding to thicknesses of 11 km, 9.5 km, and 7.5 km respectively (Fig. 20). These calculated thicknesses are far greater than any existing Proterozoic sedimentary deposit, suggesting that for these samples, the gradual cooling scenario is more likely than the reburial scenario.

For the Los Pinos Mountains and Front Range, CO locations the maximum Precambrian temperatures during reburial varies when compared to the previous samples. For the Los Pinos Mountains sample the depth of reburial ranges from 3.5 km - 9.5 km and for the Front Range, CO sample the depth of reburial ranges from 1.5 km - 11 km (Fig. 20). The minimum thickness of each is consistent with the thicknesses recorded in the existing Proterozoic sedimentary deposits.

Although, for the Front Range sample the ZHe date-eU curves in the reburial scenario do not actually match the recorded ZHe data that well compared to the ZHe date-eU curves produced in the gradual scenario model (Fig. 18). Only four of the curves actually fit all seven data points in the reburial scenario while the remaining thirteen curves only fall within the error percentage of two data points. When compared to the ZHe date-eU curves in the gradual scenario all fourteen curves are similar to one another and fall within the error percentage of all the data points (Fig. 18). Therefore, the scenario that best fits the data is the t-T paths recorded in the gradual inverse scenario model.

Overall good paths were found for both scenarios for all five samples. However, for the Tres Piedras, Santa Fe, and Sandia Mountains locations the depth of burial recoded in the reburial

inverse models suggests the presence of a sedimentary basin that is far too thick to have formed when compared to the Proterozoic sedimentary deposits that exist today (Fig. 20). Additionally, even though the Front Range, CO sample has certain t-T paths that would correspond to basins that are comparable in thickness to those recorded today the fit of the ZHe date-eU curves is not as coherent with the ZHe data points when compared to those produced in the gradual inverse models. Therefore, for the Tres Piedras, Santa Fe, Sandia Mountains, and Front Range samples the scenario that is more likely to have occurred is the gradual inverse model scenario. For all four samples the gradual inverse models imply that the samples gradually cooled after crystallization, were exhumed between 1000-800 Ma, and reached surface temperatures between 800-600 Ma (Fig. 19). The only sample where the reburial scenario remains a possibility is the Los Pinos Mountains. The ZHe date-eU curves produced fit the recorded data points, and the minimum thickness of the hypothetical basin necessary to bury the samples to the temperatures recorded is similar to the thickness of Proterozoic sedimentary deposits today. Therefore, for this sample the ZHe data are unable to distinguish between a reburial or gradual scenario.

Additionally, compiled $^{40}Ar/^{39}Ar$ data from New Mexico provides further evidence that the thermal histories implied from the gradual inverse models are valid. A density plot created from the compiled K-spar data shows that a majority of the ages fall between 1000-800 Ma with only two data points falling outside that range (Fig. 21). The data obtained from this specific mineral is important because the partial retention zones of K-spar overlap with the ZHe retention temperatures. K-spar has an upper limit of 225 °C and lower limit of 175 °C (*Reiners & Brandon* 2006) while the ZHe retention zone falls between 250-50 °C (*Guenthner et al.,* 2013; *Johnson et al*. 2015). The ages obtained from this dating method correspond to many of the older ZHe dates obtained from the samples analyzed in this study. Additionally, the results of the compiled

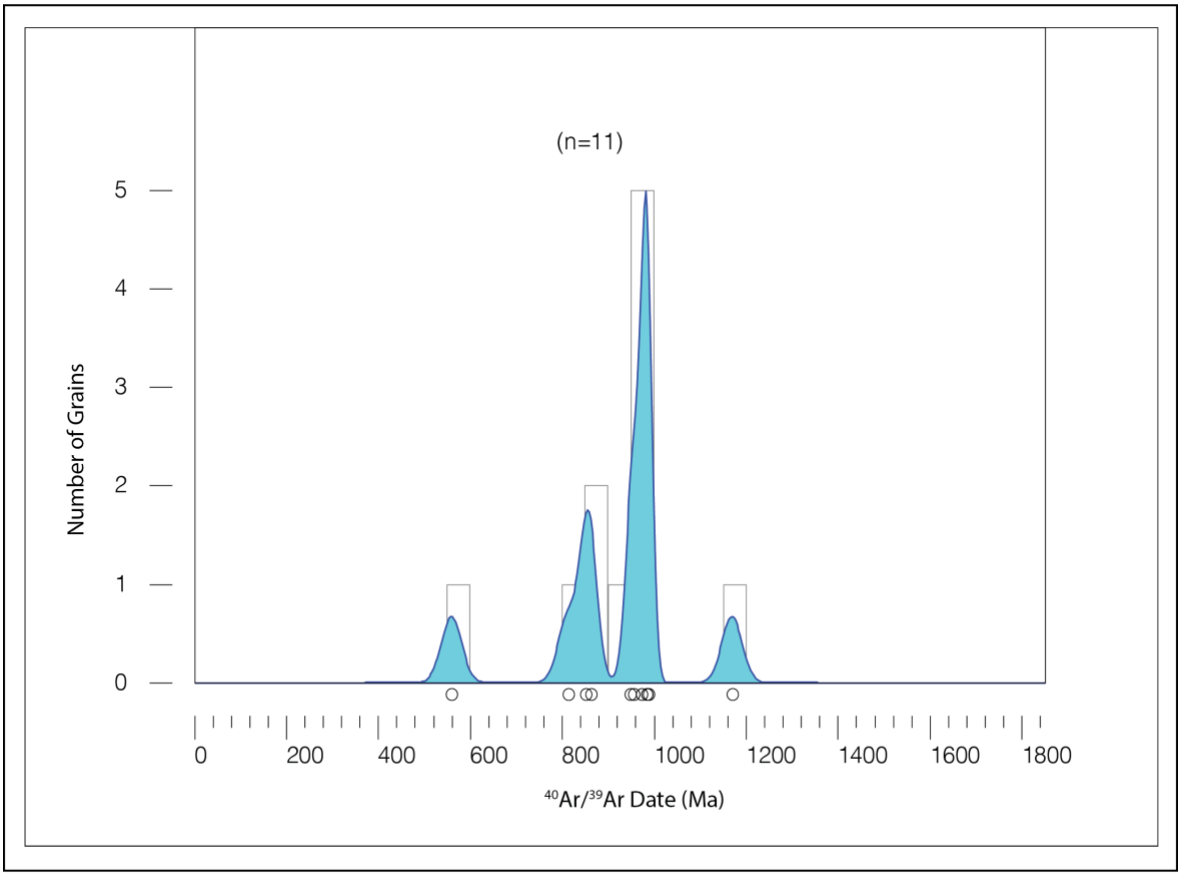

Figure 21: Density plot of compiled K-spar $^{40}Ar/^{39}Ar$ data from New Mexico and Colorado. A total of 11 ages were obtained and shown on the plot.

K-spar $^{40}Ar/^{39}Ar$ data imply that these samples must have passed through a temperature range of 225-175 °C between 1000-800 Ma, in agreement with many of the t-T paths observed in the gradual inverse models. Particularly in the Santa Fe, Tres Piedras, Sandia Mountains, and Front Range gradual inverse models t-T paths are recorded to have passed through the K-spar retention zone between 1000-800 Ma (Fig. 19). The only gradual inverse model that does not contain any paths that pass through this temperature zone between 1000-800 Ma is the Los Pinos location. For this sample the timing of exhumation seems to occur much earlier between 1400-1200 Ma (Fig. 19). With some t-T paths reaching surface temperatures by ~1200 Ma and others by ~500 Ma (Fig. 19).

Finally, when comparing the results of the gradual vs. inverse model scenarios it is clear that the gradual scenario is more likely to have occurred for the Tres Piedras, Santa Fe, Sandia Mountains, and Front Range samples. Multiple forms of evidence support this conclusion and the models imply that exhumation occurred between 1000-800 Ma and samples reached surface temperatures between 800-600 Ma (Fig. 19). For the Los Pinos Mountains sample either scenario is likely. If the reburial scenario occurred then half of the t-T paths recorded in this model imply that exhumation to surface temperatures took place between ~800-500 Ma, while the remaining t-T paths indicate that cooling could have taken place between ~400-300 Ma. However, if the gradual cooling scenario is correct, then exhumation occurred much earlier between 1400-1200 Ma when compared to the other four samples (Fig. 19).

5.2 Implications for Supercontinent Cycles

Continent-continent collisions that took place between 1.3 to 0.9 Ga constituted the final assembly of supercontinent Rodinia. The breakup of this supercontinent occurred in two main phases. The first pulse began on the western margin of Laurentia between 780-680 Ma, and the

second main phase occurred on the eastern margin between 620-550 Ma (*Whitmeyer and Karlstrom* 2007). This timing seems to overlap with the timing of exhumation and when most of the samples analyzed in this study seem to reach surface temperatures. Specifically, the timing of breakup clearly overlaps with the timing of exhumation observed in the Tres Piedras, Santa Fe, Front Range, and Sandia Mountains gradual inverse models (Fig. 19). All four of these samples record t-T paths that reach surface temperatures between 800-600 Ma. Density plots created to showcase the distribution of when individual t-T paths cooled below 40 °C reinforce this idea. For the Tres Piedras sample the pulse occurs at 29 out of 39 paths cool to temperatures <40 °C between 780-550 Ma (Fig. 19). The Santa Fe, NM sample records the main pulse at ~650 Ma and 4 out of 7 total paths fall within the timing of breakup of Rodinia. Of the three paths that do not fall within the timing of breakup two show that cooling occurs much earlier at ~950 Ma and the third shows cooling occurred much later at ~350 Ma (Fig. 19). For Front Range, CO all 14 t-T paths correlate with the breakup of Rodinia, and the main pulse of when these paths cooled below 40 °C takes place at ~600 Ma. Finally, for the Sandia Mountains the majority of paths cool at ~580 Ma and 49 out of 53 t-T paths fall between 780-550 Ma (Fig. 19).

The timing of exhumation observed in these inverse models overlaps with the deposition of certain units within the Grand Canyon Supergroup and the Pahrump Group in Death Valley. Within the Grand Canyon Supergroup, the Nankoweap Formation, Chuar Group, and Sixtymile Formation were all deposited between 800-600 Ma. Within the Pahrump Group the Horse Thief Spring Formation, Beck Spring Dolomite and Kingston Peak Formation were all also deposited between 800-600 Ma (Fig. 5). The timing of deposition of these units clearly overlaps with the main pulses of exhumation recorded in the Tres Piedras, Santa Fe, Front Range, and Sandia

Mountains samples. Further strengthening the argument that the implications gathered from these gradual inverse models are valid.

Additionally, other studies analyzing samples from various locations have correlated Precambrian exhumation with the formation and breakup of Rodinia. Thermal history modeling for the Carrizo Mountains, western Texas and Cookes Range, southern New Mexico found a correlation between pulses of uplift and continental assembly and breakup of Rodinia (*Reade* 2019). Results for the Carrizo Mountains imply that rapid uplift occurred between 1040 to 980 Ma, where the sample was cooled to surface temperatures between 1000-950 Ma (*Reade*, 2019). This period of exhumation can be correlated to the final assembly of Rodinia which occurred between 1.3-0.95 Ga (*Whitmeyer and Karlstrom* 2007). The Cookes Range sample implies two periods of uplift may have occurred between 1200-980 Ma and 800-600 Ma, which can be correlated to the assembly and breakup of Rodinia (*Reade* 2019). A separate study focused on thermal history modeling from data collected in the Ozark Plateau of Missouri that also linked the timing of Proterozoic exhumation to Rodinia breakup (*DeLucia et al*. 2017). Inverse model results from this location imply that a period of reburial throughout the Precambrian is possible, and document exhumation between 850-680 Ma. *DeLucia et al*. (2017) state that this period of exhumation recorded in their data can be correlated to the final stages of breakup of Rodinia.

Furthermore, a study from *Flowers et al.* (2020) found that exhumation observed in the Pikes Peak batholith from southern Colorado occurred sometime between ~1000 and 717 Ma. The inverse model results for this study found that the viable set of t-T paths showed rapid cooling after crystallization at ~1066 Ma and were then exhumed and reached surface temperatures between 1000-717 Ma. *Flowers et al.* (2020) link the recorded exhumation periods to either the assembly of supercontinent Rodinia or the breakup. Additionally, when comparing

the ZHe data collected from Pikes Peak to the compiled ZHe data points from all five samples a clear trend can be observed between the two data sets. Primarily a clear negative correlation between ZHe date and eU concentration is observed along with the inflection point where the highly negative slope begins to flatten occurring at an eU concentration of ~500 ppm (Fig. 22) The Pikes Peak data also contains maximum ZHe ages similar to those recorded in the Los Pinos Mountains, Santa Fe, and Sandia Mountains (Fig. 22). Overall the ZHe date and inverse model results obtained from this study are consistent and reinforce the results obtained from the five samples analyzed in this paper.

While the reburial scenario for the Los Pinos Mountains sample does contain t-T paths that show cooling that correlates with the breakup of Rodinia the gradual scenario for this sample is the only model that does not clearly correlate with the timing of breakup of this supercontinent. The gradual inverse scenario model for this sample implies that the timing of exhumation occurred much earlier between 1400-1200 Ma, with some t-T paths reaching surface temperatures by ~1200 Ma and others by ~500 Ma (Fig. 19). These recorded t-T paths could possibly be explained by Grenville-age extension that may have caused pulses of exhumation for basement rocks at depths of ~10 km between 1.45 and 1.35 Ga (*Whitmeyer & Karlstrom* 2007). This period of exhumation can be linked to erosion of a 1.4 Ga plateau, which also led to three pulses of uplift across extensional faults occurring at 1.25 Ga, 1.1 Ga, and 0.8 Ga (*Timmons et al.* 2001). Therefore, these t-T paths that show exhumation to the surface prior to Rodinia breakup in the Los Pinos models can still be explained and linked to supercontinent cycles.

Multiple forms of evidence support the gradual cooling scenario and the subsequent linking of exhumation to supercontinent cycles. For the Tres Piedras, Front Range, Sandia Mountains, and Santa Fe samples the timing of when they reach surface temperatures clearly

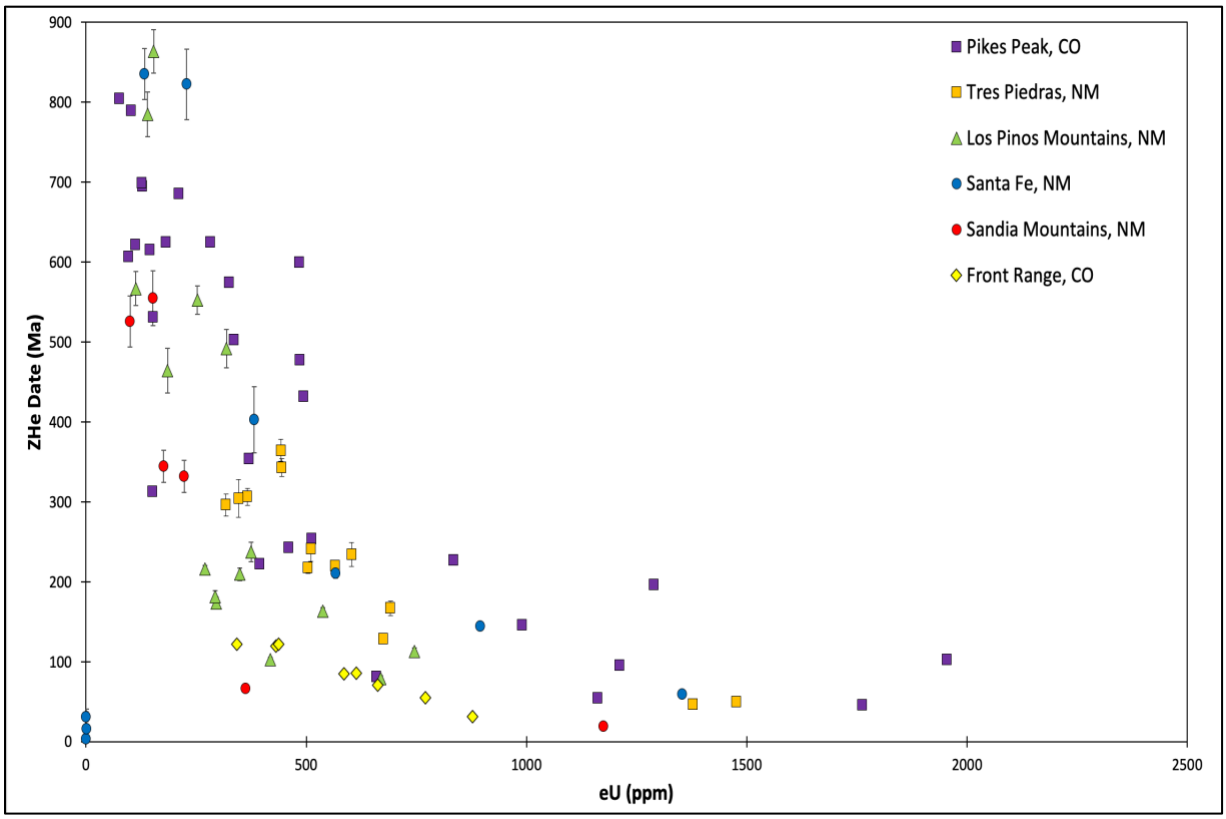

Figure 22: eU vs. zircon (U-Th)/He date plot comparison of data from Pikes Peak, CO; Tres Piedras, NM; Los Pinos Mountains, NM; Santa Fe, NM; Sandia Mountains, NM; and Front Range, CO. Date uncertainties are 2σ. [*Ault et al.* (2018); *Flowers et al.* (2020)]

overlaps with the breakup of Rodinia. For the Los Pinos sample if the gradual scenario occurred the timing of exhumation transpired much earlier. However, the exhumation period observed in this sample can still be linked to the supercontinent cycle due to Grenville-age extension that resulted in exhumation of basement rocks (*Whitmeyer & Karlstrom* 2007).

Another mechanism that may have caused the exhumation recorded in the inverse models is Snowball Earth glaciations, which occurred from 717 to 635 Ma (*Flowers et al.* 2020). This event has been proposed to have caused a worldwide denudation episode that may have led to the formation of the Great Unconformity. Although, results from the inverse models show that the main pulses of exhumation occurred either before or after this event. Figure 19 shows that the majority of t-T paths cooled to surface temperatures at ~600 Ma or younger particularly in the Tres Piedras, Santa Fe, Sandia Mountains, and Front Range models. While the Los Pinos models records older exhumation between 1400-1200 Ma (Fig. 19). Additionally, the inverse model results from *Flowers et al.* (2020) support this conclusion as well with the majority of exhumation observed in the Pikes Peak sample occurring prior to the Snowball Earth glaciation event. Based off the inverse model results from this study this event is not the strongest signal to have caused the exhumation recorded and is more likely linked to the breakup of Rodinia.

Overall the scenario that is likely to have occurred for the Santa Fe, Tres Piedras, and Sandia Mountains samples is the gradual cooling model. For the Los Pinos Mountains and Front Range, CO locations both the reburial and gradual cooling models are possible. Due to these results this indicates that two scenarios are possible for the five samples analyzed in this study. The first option would be that all five samples experienced a gradual cooling scenario. If this is true, then four out of the five samples modeled would have experienced exhumation that overlaps with the breakup of Rodinia. The only sample that does not overlap with the timing of

breakup is the Los Pinos Mountains location (Fig. 19). For this sample exhumation is recorded to have occurred much earlier compared to the other samples and could possibly be explained by Grenville-age extension that could have resulted in the exhumation of basement rocks. The second option would be that the Santa Fe, Tres Piedras, and Sandia Mountains experienced the gradual cooling scenario while the Los Pinos and Front Range samples experienced the reburial scenario. If this situation occurred, then all five samples record cooling to surface temperatures that overlaps with the breakup of Rodinia (Fig. 19).

Chapter 6: Conclusion

In total 51 new and compiled zircon (U-Th)/He dates were utilized in this study in order to constrain the long-term thermal history of Precambrian rocks in New Mexico and Colorado. New zircon grains were collected from Santa Fe, Tres Piedras, and Los Pinos Mountains and compiled data was collected from the Sandia Mountains and Front Range, CO. ZHe analysis for all five samples resulted in dates that span millions of years over a wide range of eU values. Two sets of forward models that tested various Precambrian histories were run, but none of the corresponding ZHe date-eU curves matched the data. Inverse modeling was then utilized in order to test thousands of paths to further constrain the thermal history. Two inverse model scenarios were completed for each sample including a gradual cooling and reburial scenario. While good paths were found for both scenarios the gradual cooling model is more likely to have occurred for the Tres Piedras, Santa Fe, and Sandia Mountains locations. The gradual inverse models for these samples imply that after crystallization the samples gradually cool through time and begin to reach surface temperatures between 800-600 Ma. This timing directly overlaps with the breakup of supercontinent Rodinia. For the Front Range, CO location both the reburial and gradual scenarios remain a possibility and both scenarios record exhumation that overlaps with the breakup of Rodinia. For the Los Pinos Mountains location, both the reburial and gradual scenarios are possible as well. Although, if the gradual cooling scenario occurred for this sample then the timing of exhumation transpired much earlier between 1400-1200 Ma. This earlier period of exhumation can still be linked to supercontinent cycles due to Grenville-age extension that resulted in exhumation of basement rocks. Overall the results of the inverse models indicate that two scenarios are possible for the five samples analyzed. Scenario one would be that the gradual cooling model occurred for all five locations. In this situation four out of the five samples record cooling to surface

temperatures during the breakup of Rodinia. The second option would be that only the Santa Fe, Tres Piedras, and Sandia Mountains samples experienced the gradual cooling model while the Los Pinos Mountains and Front Range locations underwent the reburial model. If this option occurred, then all five samples show exhumation that overlaps with the breakup of Rodinia. Overall the thermal histories recorded in the inverse models link the cooling to near-surface temperatures to the breakup of supercontinent Rodinia. These new data provide new and important insight into the timescales and processes of continental exhumation during assembly and break-up of supercontinents.

References

Abitz, R. J., Ward, D. B., & Brookins, D. G. (1987). Rb-Sr age for lower crust in the southern Rio Grande Rift, New Mexico. *Isochron West*, *49*, 8-12.

Aldrich, L. T., Wetherill, G. W., & Davis, G. L. (1957). Occurrence of 1350 million-year-old granitic rocks in western United States. *Geological Society of America Bulletin*, *68*(5), 655-656.

Aldrich, L. T., Wetherill, G. W., David, G. L., & Tilton, G. R. (1958). Radioactive ages of micas from granitic rocks by Rb-Sr and K-A methods. *Eos, Transactions American Geophysical Union*, *39*(6), 1124-1134.

Amato, J. M., Heizler, M. T., Boullion, A. O., Sanders, A. E., Toro, J., McLemore, V. T., & Andronicos, C. L. (2011). Syntectonic 1.46 Ga magmatism and rapid cooling of a gneiss dome in the southern Mazatzal Province: Burro Mountains, New Mexico. *Bulletin*, *123*(9-10), 1720-1744.

Amato, J. M., & Mack, G. H. (2012). Detrital zircon geochronology from the Cambrian Ordovician Bliss Sandstone, New Mexico: Evidence for contrasting Grenville-age and Cambrian sources on opposite sides of the Transcontinental Arch. *Bulletin*, *124*(11-12), 1826-1840.

Ault, A. K., Guenthner, W. R., Moser, A. C., Miller, G. H., & Refsnider, K. A. (2018). Zircon grain selection reveals (de) coupled metamictization, radiation damage, and He diffusivity. *Chemical Geology*, *490*, 1-12.

Biddle, J. (2017). Constraining times of extension in the southern rio grande rift and basin and range using apatite and zircon (U-TH)/HE thermochronology. [M.S. thesis].

Biddle, J., Ricketts, J.W., and Amato, J.M. (2018). Constraining timing of extension in the southern Rio Grande rift and Basin and Rage using apatite and zircon (U-Th)/He thermochronology, *in* Mack, G.H., Hampton, B.A., Ramos, F.C., Witcher, J.C., and Ulmer-Scholle, D.S., eds., Las Cruces Country III: New Mexico Geological Society, Guidebook 69, p. 127-135.

Brookins, D. G., Enz, R. D., Kudo, A. M., & Shafiqullah, M. (1975). K-Ar and Rb-Sr age determinations of orbicular granite. *Sandia Mountains, New Mexico: Isochron/West*, (12), 11-13.

Brookins, D. G., & Majumdar, A. (1982). The Sandia granite: single or multiple plutons. *New Mexico Geological Society Guidebook*, *33*, 221-223.

Brookins, D. G., & Shafiqullah, M. (1975). K-Ar ages for pegmatitic and metamorphic muscovites. *Sandia Mountains, New Mexico: Isochron/West*, (12), 9.

Brown, C. L., Karlstrom, K. E., Heizler, M. T., Unruh, D., Pazzaglia, F. J., & Lucas, S. G. (1999). Paleoproterozoic deformation, metamorphism, and 40Ar/39Ar thermal history of the 1.65-Ga Manzanita pluton, Manzanita Mountains, New Mexico. In *50th Annual Field Conference Guidebook* (pp. 255-268).

Cather, S.M. (2004). Laramide orogeny in central and northern New Mexico and southern Colorado. *New Mexico Geological Society, Special Publication 11*, 203-248.

Corsetti, F. A., & Hagadorn, J. W. (2000). Precambrian-Cambrian transition: Death Valley, United States. *Geology*, *28*(4), 299-302.

Dehler, C., Gehrels, G., Porter, S., Heizler, M., Karlstrom, K., Cox, G., Crossey, L., & Timmons,

M. (2017). Synthesis of the 780–740 Ma Chuar, Uinta Mountain, and Pahrump (ChUMP) groups, western USA: implications for Laurentia-wide cratonic marine basins. *Bulletin*, *129*(5-6), 607-624.

DeLucia, M. S., Guenthner, W. R., Marshak, S., Thomson, S. N., & Ault, A. K. (2017). Thermochronology links denudation of the Great Unconformity surface to the supercontinent cycle and snowball Earth. Geology, 46(2), 167-170.

Dumond, G., Mahan, K., Williams, M.W., and Karlstrom, K. E. (2007). Metamorphism in middle continental crust, Upper Granite Gorge, Grand Canyon, Arizona: Implications for segmented crustal architecture, processes at 25-km-deep levels, and unroofing of orogens: *Geological Society of America Bulletin*, *119*, 202–220.

Elston, D. P., & Scott, G. R. (1973). Paleomagnetism of some Precambrian basaltic flows and red beds, eastern Grand Canyon, Arizona. *Earth and Planetary Science Letters*, *18*(2), 253-265.

Erslev, E. A., Fankhauser, S. D., Heizler, M. T., Sanders, R. E., Cather, S. M., & Nelson, E. P. (2004). Strike-slip tectonics and thermochronology of northern New Mexico: A field guide to critical exposures in the southern Sangre de Cristo Mountains. *Field Trips in the Southern Rocky Mountains: Boulder, Colorado, Geological Society of America, Field Guide*, *5*, 15-40.

Farley, K. A., Wolf, R. A., & Silver, L. T. (1996). The effects of long alpha-stopping distances on (U-Th)/He ages. *Geochimica et cosmochimica acta*, *60*(21), 4223-4229.

Flowers, R. M., Macdonald, F. A., Siddoway, C. S., & Havranek, R. (2020). Diachronous development of Great Unconformities before Neoproterozoic Snowball Earth. *Proceedings of the National Academy of Sciences*.

Gable, D. J. (1972). *Geologic map of the Tungsten Quadrangle, Boulder, Gilpin, and Jefferson Counties, Colorado* (No. 978).

Giffin, C. E., & Kulp, J. L. (1960). Potassium-argon ages in the Precambrian basement of Colorado. *Bull. Geol. Soc. Am.*, *71*.

Goldich, S. S., Lidiak, E. G., Hedge, C. E., & Walthall, F. G. (1966). Geochronology of the midcontinent region, United States: 2. Northern area. *Journal of Geophysical Research*, *71*(22), 5389-5408.

Grambling, J. A., & Dallmeyer, R. D. (1993). Tectonic evolution of Proterozoic rocks in the Cimarron Mountains, northern New Mexico, USA. *Journal of Metamorphic Geology*, *11*(5), 739-755.

Gresens, R. L. (1975). Geochronology of Precambrian metamorphic rocks, north-central New Mexico. *Geological Society of America Bulletin*, *86*(10), 1444-1448.

Guenthner, W. R., Reiners, P. W., Ketcham, R. A., Nasdala, L., & Giester, G. (2013). Helium diffusion in natural zircon: Radiation damage, anisotropy, and the interpretation of zircon (U-Th)/He thermochronology. *American Journal of Science*, *313*(3), 145-198.

Hansen, W. R., & Peterman, Z. E. (1968). Basement-rock geochronology of the Black Canyon of the Gunnison, Colorado. *US Geological Survey Professional Paper*, *400*, C80-C90.

Harbour, R. L. (1960). Precambrian rocks at North Franklin Mountain, Texas. *AAPG Bulletin*, *44*(11), 1785-1792.

Hedlund D.C. (1978a). Geologic map of the Gold Hill Quadrangle, Grant County, New Mexico: *U.S. Geological Survey Miscellaneous Field Studies*, Map MF-1035, scale 1:24,000.

Hedlund D.C. (1978b). Geologic map of the Werney Hill quadrangle, Grant County, New

Mexico: *U.S. Geological Survey Miscellaneous Field Studies*, Map MF-1038, scale 1:24,000.
Hedlund D.C. (1980). Geologic map of the Redrock NE quadrangle, Grant County, New Mexico: *U.S. Geological Survey Miscellaneous Field Studies* Map MF-1264, scale 1:24,000.
Hoffman, P. F., Kaufman, A. J., Halverson, G. P., & Schrag, D. P. (1998). A Neoproterozoic snowball earth. *science*, *281*(5381), 1342-1346.
House, M.A., Kelley, S.A., and Roy, M. (2003). Refining the footwall cooling history of a rift flank uplift, Rio Grande rift, New Mexico. *Tectonics, 22,* 1060-1078.
Johnson, J. E. (2015). ""Inverted" Zircon and Apatite (U-Th)/He Dates and Interpretation of High-Damage Zircon from the Southern Rocky Mountains, Front Range, Colorado". Geological Sciences Graduate Theses & Dissertations. 114.
Johnson, R. B., & Read, C. B. (1952). Stratigraphy of Paleozoic, Mesozoic rocks in parts of central New Mexico. *New Mexico Geological Society*, 106-126.
Karlstrom, K.E., Amato, J.M., Williams, M.L., Heizler, M., Shaw, C., Read, A., and Bauer, P., (2004). Proterozoic tectonic evolution of the New Mexico region: a synthesis. *New Mexico Geological Society Special Publication, 11*, 1-34.
Karlstrom, K. E., Dallmeyer, R. D., & Grambling, J. A. (1997). 40Ar/39Ar evidence for 1.4 Ga regional metamorphism in New Mexico: Implications for thermal evolution of lithosphere in the southwestern USA. *The Journal of Geology*, *105*(2), 205-224.
Karlstrom, K., Hagadorn, J., Gehrels, G., Matthews, W., Schmitz, M., Madronich, L., Mulder, J., Pecha, M., Giesler, D., & Crossey, L. (2018). Cambrian Sauk transgression in the Grand Canyon region redefined by detrital zircons. *Nature Geoscience*, *11*(6), 438-443.
Karlstrom, K.E., and Timmons, J. M. (2012). Many unconformities make one 'Great Unconformity'. *Geological Society of America Special Paper*. *489*, 73-79.
Karlstrom, K.E., Heizler, M., Mohr, M.T., Schmitz, M., Timmons, J.M., Crossey, L.J., Hagadorn, J., & Dehler, C. (2019). Parsing Grand Canyon's Great Unconformities. *In review*.
Kelley, S. A., Chapin, C. E., & Corrigan, J. (1992). Late Mesozoic to Cenozoic cooling histories of the flanks of the northern and central Rio Grande rift, Colorado and New Mexico. *New Mexico Bureau of Mines & Mineral Resources*. *145*.
Kelley, S.A., and Chapin, C.E. (2004). Denudation history and internal structure of the Front Range and Wet Mountains, Colorado, based on apatite fission track thermochronology. *Geological and Mineralogical Resources Bulletin. 160,* 41-78.
Kelley, V.C., and Northrop, S.A. (1975). Geology of Sandia Mountains and vicinity, New Mexico. *New Mexico Bureau of Mines and Mineral Resources Memoir. 29*, 136.
Ketcham, R. A., (2005). Forward and inverse modeling of low-temperature thermochronometry data. *Reviews in mineralogy and geochemistry, 58*(1), 275- 314.
Kirby, E., Karlstrom, K. E., Andronicos, C. L., & Dallmeyer, R. D. (1995). Tectonic setting of the Sandia pluton: An orogenic 1.4 Ga granite in New Mexico. *Tectonics, 14*(1), 185-201.
Mahon, R. C., Dehler, C. M., Link, P. K., Karlstrom, K. E., & Gehrels, G. E. (2014). Detrital zircon provenance and paleogeography of the Pahrump Group and overlying strata, Death Valley, California. *Precambrian Research*, *251*, 102-117.
Mahon, R. C., Dehler, C. M., Link, P. K., Karlstrom, K. E., & Gehrels, G. E. (2014).

Geochronologic and stratigraphic constraints on the Mesoproterozoic and Neoproterozoic Pahrump Group, Death Valley, California: A record of the assembly, stability, and breakup of Rodinia. *Bulletin*, *126*(5-6), 652-664.

Marcoline, J. R., Heizler, M. T., Goodwin, L. B., Ralser, S., & Clark, J. (1999). Thermal, structural, and petrological evidence for 1400-Ma metamorphism and deformation in central New Mexico. *Rocky Mountain Geology*, *34*(1), 93-119.

Marcoline, J. R., Ralser, S., & Heizler, M. T. (1995). Monte Largo shear zone Manzano Mountains New Mexico: Tectonic significance and argon geochronology. *New Mexico Geology*, *17*, 26.

Marvin, R. F., & Dobson, S. W. (1979). Radiometric ages: compilation B. *US Geological Survey: Isochron/West*, *26*, 3-32.

Muehlberger, W. R., & Denison, R. E. (1964). Precambrian geology of south-central New Mexico. In *Guidebook, 15th Field Conf., Ruidoso County, New Mexico: New Mexico Geol. Soc* (pp. 62-69).

Muehlberger, W. R., Hedge, C. E., Denison, R. E., & Marvin, R. F. (1966). Geochronology of the midcontinent region, United States: 3. Southern area. *Journal of geophysical research*, *71*(22), 5409-5426.

Pedrick, J. (1995). Polyphase proterozoic tectonometamorphic history of the Taos Range, northern New Mexico.

Peterman, Z. E., & Hedge, C. E. (1968). Chronology of Precambrian events in the Front Range, Colorado. *Canadian Journal of Earth Sciences*, *5*(3), 749-756.

Peters, S. E., & Gaines, R. R. (2012). Formation of the 'Great Unconformity' as a trigger for the Cambrian explosion. *Nature*, *484*(7394), 363.

Premo, W.R., and Fanning, C.M. (2000). SHRIMP U-Pb zircon ages for Big Creek gneiss, Wyoming and Boulder Creek batholith, Colorado: implications for timing of Paleoproterozoic accretion of the northern Colorado province. *Rocky Mountain Geology 35*, 31-50.

Read, A.S., Koning, D.J., Smith, G.A., Ralser, S., Rogers, J., Bauer, P.W., (2000). Geology of the Santa Fe 7.5-min. quadrangle, Santa Fe County, New Mexico. *New Mexico Bureau of Mines and Mineral Resources,* Open-file Geologic Map OF-GM 32, scale 1:12,000.

Reiners, P. W., & Brandon, M. T. (2006). Using thermochronology to understand orogenic erosion. *Annual Rev. Earth Planet. Sci.*, *34*, 419-466.

Reiners, P. W., & Ehlers, T. A. (Eds.). (2018). *Low-Temperature Thermochronology: Techniques, Interpretations, and Applications* (Vol. 58). Walter de Gruyter GmbH & Co KG.

Reiners, P. W. (2005). Zircon (U-Th)/He thermochronometry. *Reviews in Mineralogy and Geochemistry*, *58*(1), 151-179.

Rice, C. M., Lux, D. R., & Macintyre, R. M. (1982). Timing of mineralization and related intrusive activity near Central City, Colorado. *Economic Geology*, *77*(7), 1655-1666.

Ricketts, J.W., Kelley, S.A., Karlstrom, K.E., Schmandt, B., Donahue, M.S., and van Wijk, J. (2015). Synchronous opening of the Rio Grande rift along its entire length at 25-10 Ma supported by apatite (U-Th)/He and fission-track thermochronology, and evaluation of possible driving mechanisms. *Geological Society of America Bulletin 128*, 397-424.

Sanders, R. E., Heizler, M. T., & Goodwin, L. B. (2006). 40Ar/39Ar thermochronology

constraints on the timing of Proterozoic basement exhumation and fault ancestry, southern Sangre de Cristo Range, New Mexico. *Geological Society of America Bulletin*, *118*(11-12), 1489-1506.

Shastri, L. L., & Bowring, S. A. (1992). Timing of Proterozoic deformation, plutonism, and metamorphism in the Los Pinos Mountains, central New Mexico. *Geological Society of America, Abstracts with Programs;(United States)*, *24*(CONF-921058--).

Shaw, C. A., Heizler, M. T., Karlstrom, K. E., & Keller, G. R. (2005). 40Ar/39Ar thermochronologic record of 1.45–1.35 Ga intracontinental tectonism in the southern Rocky Mountains: Interplay of conductive and advective heating with intracontinental deformation. *The Rocky Mountain Region–An Evolving Lithosphere: Tectonics, Geochemistry, and Geophysics. American Geophysical Union, Geophysical Monograph*, *154*, 163-184.

Shaw, C. A., Snee, L. W., Selverstone, J., & Reed, Jr, J. C. (1999). 40Ar/39Ar thermochronology of Mesoproterozoic metamorphism in the Colorado Front Range. *The Journal of Geology*, *107*(1), 49-67.

Shride, A.F. (1967). Younger Precambrian Geology in Southern Arizona. *U.S. Geological Survey Professional Paper, 566(88).*

Soegaard, K., & Callahan, D. M., (1994). Late middle Proterozoic Hazel Formation near Van Horn, Trans-Pecos Texas: Evidence for transpressive deformation in Grenvillian basement. *Geological Society of America Bulletin, 106*(3), 413-423.

Spiegel, Z., Baldwin, B., Kottlowski, F. E., Barrows, E. L., & Winkler, H. A. (1963). Geology and water resources of the Santa Fe area, New Mexico. *Geological Survey Water-Supply Paper, 1525*.

Stewart, J.H., Gehrels, G.E., Barth, A.P., Link, P.K., Christie-Blick, N., & Wrucke, C.T. (2001). Detrital zircon provenance of Mesoproterozoic to Cambrian arenites in the western United States and northwestern Mexico. *Geological Society of America Bulletin, 113*, 1343–1356.

Thomann, W. F. (1981). Ignimbrites, trachytes, and sedimentary rocks of the Precambrian Thunderbird Group, Franklin Mountains, El Paso, Texas. *Geological Society of America Bulletin*, *92*(2), 94-100.

Thompson, A. G., Grambling, J. A., & Dallmeyer, R. D. (1991). Proterozoic tectonic history of the Manzano Mountains, central New Mexico. *New Mexico Bureau of Mines and Mineral Resources Bulletin*, *137*, 71-77.

Thompson, A. G., Grambling, J. A., Karlstrom, K. E., & Dallmeyer, R. D. (1996). Mesoproterozoic metamorphism and 40Ar/39Ar thermal history of the 1.4 Ga Priest pluton, Manzano Mountains, New Mexico. *The Journal of Geology*, *104*(5), 583-598.

Timmons, J. M., Karlstrom, K. E., Dehler, C. M., Geissman, J. W., & Heizler, M. T. (2001). Proterozoic multistage (ca. 1.1 and 0.8 Ga) extension recorded in the Grand Canyon Supergroup and establishment of northwest-and north-trending tectonic grains in the southwestern United States. *GSA Bulletin*, *113*(2), 163-181.

Timmons, J. M., Karlstrom, K. E., Heizler, M. T., Bowring, S. A., Gehrels, G. E., & Crossey, L. J. (2005). Tectonic inferences from the ca. 1255–1100 Ma Unkar Group and Nankoweap Formation, Grand Canyon: Intracratonic deformation and basin formation during protracted Grenville orogenesis. *Geological Society of America Bulletin*, *117*(11-12), 1573-1595.

Timmons, J. M., Bloch, J., Fletcher, K., Karlstrom, K. E., Heizler, M., & Crossey, L. J.

(2012). The Grand Canyon Unkar Group: Mesoproterozoic basin formation in the continental interior during supercontinent assembly. *GSA Special Paper*, *489*, 25- 47.
Wobus, R. A. (1984). An overview of the Precambrian geology of the Tusas Range, north central New Mexico. In *New Mexico Geological Society Guidebook 35th Field Conference, Rio Grande Rift: Northern New Mexico* (pp. 193-198).
Woldegabriel, G. (1990). Hydrothermal alteration in the Valles caldera ring fracture zone and core hole VC-1: evidence for multiple hydrothermal systems. *Journal of Volcanology and Geothermal Research*, *40*(2), 105-122.

Vita

Jacoup Roiz was born and raised in Eagle Pass, TX. He attended Eagle Pass High School where he completed the GeoForce scholar program and received his diploma in 2014. Upon graduation he pursued a Bachelor of Science in Geological Sciences degree at The University of Texas at Austin and earned the GeoForce student scholarship. While pursuing his bachelor's degree he also worked as a research assistant under the guidance of Dr. Whitney Behr and Dr. Robert Porritt and completed his senior thesis his senior year. Jacoup then enrolled in the Master of Science in Geological Sciences program in 2018 at UTEP. While completing his Masters, Jacoup also worked as a research assistant for Dr. Jason Ricketts and a teaching assistant for Historical Geology, Introduction to Physical Geology, and Physical Geography between fall 2018 and spring 2020. Aside from working towards his master's degree Jacoup also competed the Geographic Information Science and Technology graduate certificate in December 2019 at UTEP. Additionally, Jacoup presented his research work at the 2020 department Colloquium. Jacoup was awarded the West Texas Geological Society Scholarship, UTEP Graduate School Scholarship, and George B. McBride Graduate Fellows Scholarship for the 2019-2020 school year. He was also chosen as a Diana Natalicio Environmental Intern for summer 2019 and worked at the United States Environmental Protection Agency. Jacoup completed and received his Master of Science in Geological Sciences degree in May 2020.

Contact Information: jacouproiz@gmail.com